Yang, H., Liu, F., and Gardner, L. (2015). Post-fire behaviour of slender reinforced concrete columns confined by circular steel tubes. Thin-Walled Structures. **87**, 12-29.

Post-fire behaviour of slender reinforced concrete columns confined by circular steel tubes

Hua Yang [a,b], Faqi Liu [b,c], Leroy Gardner [c]

[a] Key Lab of Structures Dynamic Behavior and Control (Harbin Institute of Technology), Ministry of Education, Heilongjiang, Harbin, 150090, China

[b] School of Civil Engineering, Harbin Institute of Technology, Heilongjiang, Harbin, 150090, China

[c] Department of Civil and Environmental Engineering, South Kensington Campus, Imperial College London, SW7 2AZ, UK

Abstract:

The post-fire behaviour of slender reinforced concrete columns confined by circular steel tubes is investigated experimentally and numerically in this paper. Experiments were performed firstly to explore the fundamental behaviour of steel tube confined reinforced concrete (STCRC) slender columns after exposure to the ISO-834 standard fire, including the cooling phase. Temperature distributions, load versus lateral displacement curves, strains in the steel tube and failure modes were obtained and discussed. Next, a 3D finite element model was developed with the program ABAQUS using a sequentially coupled thermal-stress analysis. After validation of the FE model, parametric studies were carried out to identify the influence of key parameters on the load-bearing capacity and buckling reduction factor of slender STCRC columns. The considered parameters were the heating time, cross-sectional dimension, slenderness ratio, material strength, steel tube to concrete area ratio and reinforcement ratio. Finally, a simplified design method was proposed for predicting load-bearing capacity of STCRC slender columns after exposure to standard fires.

Key words: circular steel tube confined reinforced concrete; experiments; post-fire; residual capacity; slender column; testing thermal distribution

Nomenclature

A_b	cross-sectional area of reinforcing bars
A_c	cross-sectional area of concrete core
A_s	cross-sectional area of steel tube
A	cross-sectional area of composite section, $A = A_s + A_c + A_b$
d_s	diameter of bars
D	outer diameter of the steel tube
E_b	Young's modulus of reinforcement at ambient temperature
E_{bT}	Young's modulus of reinforcement after fire exposure
E_c	Young's modulus of concrete at ambient temperature
E_{cT}	Young's modulus of concrete after fire exposure
E_s	Young's modulus of structural steel at ambient temperature
E_{sT}	Young's modulus of structural steel after fire exposure
f_b	yield strength of reinforcement at ambient temperature
f_{bu}	ultimate tensile strength of reinforcement
f_{bT}	yield strength of reinforcement after fire exposure
f_{ck}	characteristic concrete strength, $f_{ck}=0.67\,f_{cu}$
f_{cu}	concrete cube strength
$f_{cu,28}$	concrete cube strength at 28 days
$f_{cu,test}$	concrete cube strength at the test day of the specimens
f_c'	concrete cylinder strength

f_{cT}'	concrete cylinder strength after fire exposure
f_{tT}'	concrete tensile strength after fire exposure
f_{su}	ultimate tensile strength of structural steel
f_y	yield strength of structural steel at ambient temperature
f_{yT}	yield strength of structural steel after fire exposure
k	factor accounting for the delay of temperature rise of concrete
L	length of column
L_e	effective length of column
N_e	load-bearing capacity of slender composite column
N_u	cross-sectional capacity of composite column
t_h	heating time to the maximum fire temperature
t_s	wall thickness of the steel tube
T	temperature
T_{max}	the maximum temperature achieved during the heating and cooling phases
α_b	ratio of reinforcement, $\alpha_b=A_b/(A_c+A_b)$
α_s	steel tube to concrete area ratio, $\alpha_s=A_s/A_c$
λ	slenderness ratio, $\lambda=L_e/i$, where i is the radius of gyration
v_s	Poisson's ratio of structural steel
ξ	confinement factor, $\xi= f_y A_s/f_{ck} A_c$
χ	buckling reduction factor

1. Introduction

Steel tube confined reinforced concrete (STCRC) columns differ from conventional concrete-filled steel tubular (CFST) columns in that steel tubes in STCRC columns are terminated at the beam to column connections (Fig.1). Thus, the steel tube does not directly bear longitudinal force and acts primarily as hoop reinforcement to the concrete, maximising the confinement and minimising the possibility of local buckling of the steel tube. Furthermore, the connections between reinforced concrete beams and STCRC columns can be designed and constructed following methods for conventional reinforced concrete structures, avoiding the complexities associated with connecting reinforced concrete beams to CFST columns.

Plain concrete columns confined by steel tubes were initially used by Gardner and Jacobson [1], Orito et al. [2], Prion and Boehme [3], O'Shea and Bridge [4,5] and Fam et al. [6], as a means of loading CFST columns. The concept of steel tube confined reinforced concrete columns as a structural member was first proposed by Tommi and his research group [7-9], with the aim of preventing shear failure and improving the ductility of reinforced concrete stub columns or boundary reinforced concrete columns in shear walls. This kind of member has subsequently attracted increasing research interest, most of which has focused on axial compressive behaviour [10,11] and seismic performance [12-14].

To date, no research has been reported on the response of STCRC columns subjected to elevated temperatures. Hence, the focus of the present investigation is the fire and post-fire behaviour of STCRC columns. Building upon the recently reported work by the authors on the post-fire behaviour of STCRC stub columns [15], this second paper examines the post-fire behaviour of STCRC slender

columns.

Experimental and numerical studies were performed to investigate the behaviour of STCRC slender columns following exposure to the ISO-834 standard fire conditions [16]. The temperatures of the furnace, the steel tube, the reinforcing bars and the concrete core were monitored and recorded during the heating and cooling phases. The load versus displacement curves, the strains in the steel tube and failure modes were obtained in the subsequent compression tests. A 3D finite element (FE) model was developed using the program ABAQUS with a sequentially coupled thermal-stress analysis, and validated against the test results. Parametric studies were then performed based on the validated FE model to identify the influence of key parameters on the residual capacity of the columns, post-fire. Finally, a simplified design method was proposed for predicting the load-bearing capacity of STCRC slender columns after fire exposure.

2. Experimental study

2.1 Specimens

A total of 14 STCRC slender columns were prepared and tested in this study. The investigation parameters were heating time (the time corresponding to the maximum furnace temperature), cross-section diameter, slenderness ratio and compressive strength of concrete. For the circular steel tube confined reinforced concrete columns, the slenderness ratio (λ) is defined as follows:

$$\lambda = \frac{L_e}{i} = \frac{4L_e}{D} \tag{1}$$

where L_e is the effective length of the column, i is the radius of gyration and D is the outer diameter of the steel tube.

Details of the test specimens are shown in Table 1, in which t_s is the thickness of the steel tube, α_s is

the steel tube to concrete area ratio ($\alpha_s=A_s/A_c$), L is the length of the specimens, α_b is the reinforcement ratio ($\alpha_b= A_b/(A_b+A_c)$) and t_h is the heating time. Each specimen is labelled according to its cross-section diameter, length to diameter ratio, nominal concrete cube compressive strength and heating time. Consider specimen C250-6-30-60, for example; C represents the composite column, 250 is the cross-section diameter in mm, 6 is the length to diameter ratio, 30 is the nominal concrete cube compressive strength in N/mm^2 and 60 is the heating time in minutes. The steel tube to concrete area ratio and reinforcement ratio were maintained approximately constant for all test specimens, with nominal values of 3.62% and 3.98%, respectively.

Two end plates, with a thickness of 10 mm, were welded to the top and bottom ends of each test specimen. Two strips with a width of 10 mm were cut from the steel tube, 100 mm away from the both end plates. These 10 mm gaps were introduced to prevent the steel tube from directly bearing longitudinal force. Six longitudinal reinforcing bars were tied at 200 mm intervals with 8 mm diameter stirrups. The concrete cover from the perimeter of the reinforcing bars to the edge of the concrete was 20 mm. A typical cross-section is shown in Fig.2.

Three STCRC stub columns were fabricated to measure temperature distributions in the specimens during the heating and cooling phases. Two of these columns had an outer diameter of 250 mm while the third had an outer diameter of 200 mm. These specimens are referred to as C250-30min, C250-60min and C200-30min, respectively. The steel tube, core concrete, reinforcing bars and stirrups of the three stub columns were the same as those in the corresponding test specimens. All three columns were 500 mm in length. Type K chromel-alumel thermocouples, with a diameter of 1.0 mm, were used to measure the temperatures of the steel tube, reinforcing bars and core concrete

at several locations in different cross-sections of the columns. At the top level (150 mm away from the top end plate), the temperatures were measured with five thermocouples (labelled 1 to 5) along the length of one axis of the cross-sections (Fig.3 (a) and (c)). The same layouts of thermocouples (labelled 6 to 10) were used at the bottom level (150 mm away from the bottom end plate), but two additional thermocouples (labelled 11 and 12) were also installed on two reinforcing bars (Fig.3 (b) and (d)).

The steel tubes in all specimens were cold formed from steel plates by press bending and seam welding. The steel tubes and reinforcing bars used for the STCRC slender columns were the same as those used for the STCRC stub columns tested in [15]. The mechanical properties of the steel after heating to 0 min, 30 min and 60 min were determined by tensile coupon testing, reported in [15] and conducted according to the Chinese Standard GB/T228-2010 [17]. The results are shown in Table 2, in which t_s is the thickness of the coupon, t_h is the heating time, E_s is the elastic modulus, f_y is the yield strength, f_{su} is the ultimate tensile strength and v_s is the Poisson's ratio. The measured stress-strain curves of the steel matches closely with the elastic-perfectly plastic stress-strain relationship up to 3.5% and 4.0% for the unexposed and exposed conditions [15], respectively, neither of which were achieved during the specimen testing. Therefore the elastic-perfectly plastic stress-strain relationship will be employed in later analysis. The results of tensile coupon tests conducted on the reinforcing bars and stirrups [15] are presented in Table 3, in which d_s is the diameter of the bars, E_b is the elastic modulus, f_b is the yield strength and f_{bu} is the ultimate tensile strength.

Concrete cubes (150 mm × 150 mm × 150 mm) and prisms (150 mm × 150 mm ×300 mm) were cast

with the same batch of concrete as used in the test specimens to determine the concrete properties. The concrete cube compressive strength f_{cu} and elastic modulus E_c at 28 days after pouring and at the test day of the specimens are shown in Table 4.

2.2 Test setup and procedure

The experiments were conducted in a specially built furnace for testing structural members at Harbin Institute of Technology, which can provide combined actions of elevated temperatures and structural loads. The floor area of the furnace is 4.9 m × 2.6 m and its height is 4.05 m. Furnace temperatures and pressures can be controlled automatically. More details can be found in [15].

The furnace temperature was increased following the ISO-834 standard fire curve including the cooling phase [16]. Before the tests, the ambient temperature was 16 ^{o}C and 21 ^{o}C for the 30 minutes' heating and 60 minutes' heating, respectively. The specimens were heated in an unstressed condition, which is considered to be more conservative than under load, when assessing the residual strength of concrete after fire exposure [18-23]. The top and bottom end plates were fully protected with ceramic fibre blankets for all specimens, including the stub columns used for measuring temperatures. This was to ensure that no heat was transferred into the specimens via the end plates. The temperatures of the steel tube, reinforcing bars and concrete were monitored and recorded with the installed thermocouples.

After cooling to ambient temperature, the specimens were loaded axially using a 5000 kN hydraulic compression machine. Pinned end conditions were achieved through a combination of a knife edge and a grooved steel plate, shown in Fig.4. The knife edge was fixed to the loading plate of the compression machine, while the steel plate with grooves was fixed to the end plate of the columns.

The columns could therefore only rotate freely about one axis. The weld seam of the outer steel tube was orientated to coincide with the centroidal axis of the column, to minimise its influence on the behaviour of the columns. The thickness of the steel plate at the location of grooves was t_e=55.2 mm; the effective length, L_e of the test specimens can therefore be calculated as $L_e=L+2t_e+2\times10$ mm, where L is the length of columns and 10 mm is the thickness of the end plates. Linear variable displacement transducers (LVDTs) were placed along the length of the column to measure the lateral displacements, as shown in Fig.4. Longitudinal and transverse strain gauges were installed on the surface of the steel tube at the mid-height of the columns to monitor the longitudinal and transverse strains.

2.3 Test results and discussions

All tested STCRC slender columns failed by global buckling, with evidence of local buckling in the most heavily compressed region of the steel section in some cases. Fig.5 presents failure modes for a typical group of columns after heating to 0 min, 30 min and 60 min. Although some crushing occurred in the concrete, the core concrete remained largely intact due to the confinement of outer steel tube, as shown in Fig.6.

The measured furnace temperatures are depicted in Fig.7, and show close agreement with the ISO-834 standard fire curve [16]. When the furnace temperatures decreased to below about 200 ^{o}C, they exceeded the control temperature slightly, though all gas burners had been turned off. This phenomenon can be attributed to the heat emitted from the furnace insulation materials and specimens. Fig.8 shows the measured temperatures in test specimens during the heating and cooling phases. Some temperatures are missing because the corresponding thermocouples failed during the

test, including thermocouple 9 on specimen C250-30min, thermocouple 12 on specimen C250-60min and thermocouples 2, 3, 4, 8 and 9 on specimen C200-30min. The maximum temperatures achieved at any stage of the heating and cooling phases decreased from the outer surface to the centre of the cross-section, but, the time corresponding to the maximum temperatures increased noticeably. For the specimen C250-30min, the average maximum temperatures of the steel tube, reinforcing bar and concrete centre were 617 ºC, 369 ºC and 258 ºC, respectively, while the corresponding times were 36.5 min, 63.7 min and 151.2 min, respectively. This delay in temperature rise was also observed in [15] and can be attributed to the high thermal capacity of the concrete and to the protection afforded by the surrounding materials. Temperature uniformity along the longitudinal direction of the test specimens was generally achieved, as may be seen in Fig.8, in which the corresponding pairs of temperatures, e.g. from thermocouples 1 and 6, are in close agreement.

The load versus mid-height lateral deflection responses of all specimens are shown in Fig.9. The graphs show that longer fire exposure times and hence higher temperatures result in lower post-fire load-bearing capacities and more rounded load-deformation behaviour. Both are primarily attributed to the change in the material stress-strain characteristics during fire exposure.

The influences of slenderness ratio, determined according to Eq.(1), on the load versus lateral displacement curves are presented in Fig.10. It can be seen that higher peak loads are obtained by the members with the smaller slenderness ratios, but this is accompanied by a more rapid post-peak decline in load-bearing capacity. This phenomenon is more prominent in the case of the columns filled with the higher strength concrete, as shown in Fig.10 (d), (e) and (f). As expected, higher load-bearing capacities can be obtained with higher strength concrete, but, regardless of fire

exposure, the post-peak unloading response becomes steeper (Fig.11).

Typical longitudinal strains in the steel tube, illustrated for the C250-6-30 specimens, at the extreme compressive and tensile fibres, are shown in Fig.12. As can be seen, the entire cross-section is under compression up to the peak load and the longitudinal strain distribution remains fairly uniform. Post-peak, the strains in part of the cross-section reverse from compression to tension, owing to the second order bending.

3. Finite element analysis

To supplement the experimental results, and to investigate further the behaviour of STCRC slender columns after fire exposure, a 3D finite element (FE) model was developed using the program ABAQUS. A transient heat transfer analysis was firstly performed to identify the thermal distributions, and then the thermal results were imported into a subsequent stress analysis.

3.1 Heat transfer analysis

The thermal response of STCRC columns under fire exposure is a transient heat transfer process, in which heat is transmitted from fire to the outer surface of the steel tube by convection and radiation and then conducted into the concrete. In this study, the convection heat transfer coefficient and resultant emissivity was defined to be 25W/(m^2K) and 0.5, respectively. The steel tube and concrete cannot be perfectly in contact during the fire exposure, therefore a constant gap conductance was defined to account for the thermal resistance at the interface, taken as 100 W/(m^2K), which has been found to produce accurate predictions of temperature [15,24-26]. The ISO-834 standard fire curve [16], including the cooling phase, was applied as the thermal load, and the ambient temperature was defined to be 20 ^{o}C.

The thermal properties of the steel and concrete, including the density, thermal conductivity and specific heat capacity, were defined based on the models proposed by Lie [27]. The influences of moisture on the thermal properties of concrete were also considered [28] and the water content was assumed to be 5% by weight.

In the FE model, the steel tube was modelled with the 4-noded shell elements (DS4), and the concrete and reinforcing bars were modelled with 8-noded continuum solid elements (DC3D8) and 2-noded truss elements (DC1D2), respectively.

3.2 Stress analysis

3.2.1 Material properties

An elastic, perfectly-plastic model was adopted to represent the material stress-strain response of the steel tube and the reinforcing bars; this model has been shown to be capable of accurately predicting the behaviour of such components in STCRC stub columns after fire exposure [15]. This model is given as follows:

$$\sigma = \begin{cases} E_{\mathrm{sT}}\varepsilon & \varepsilon \le \varepsilon_{\mathrm{yT}} \\ f_{\mathrm{yT}} & \varepsilon > \varepsilon_{\mathrm{yT}} \end{cases} \tag{2}$$

where E_{sT} and f_{yT} are the elastic modulus and yield strength of structural steel after fire exposure, respectively, and $\varepsilon_{\mathrm{yT}}$ is the residual yield strain, defined as $\varepsilon_{\mathrm{yT}} = f_{\mathrm{yT}} / E_{\mathrm{sT}}$. For the reinforcing bars, E_{sT} and f_{yT} should be replaced by E_{bT} and f_{bT}, respectively.

The residual elastic modulus and yield strength of the structural steel and reinforcing bars were determined based on the work of Tao et al. [29], as follows:

The residual elastic modulus E_{sT} for structural steel was taken as:

$$E_{sT}=\begin{cases}E_s & T_{max}\le 500^{o}\mathrm{C}\\ [1-1.30\times10^{-4}(T_{max}-500)]E_s & T_{max}>500^{o}\mathrm{C}\end{cases} \tag{3}$$

The residual elastic modulus E_{bT} for reinforcing bars can be determined by substituting E_{bT} and E_b for E_{sT} and E_s respectively into Eq.(3).

The residual yield strength f_{yT} for the structural steel was taken as:

$$f_{yT}=\begin{cases}f_y & T_{max}\le 500^{o}\mathrm{C}\\ [1-2.33\times10^{-4}(T_{max}-500)-3.88\times10^{-7}(T_{max}-500)^2]f_y & T_{max}>500^{o}\mathrm{C}\end{cases} \tag{4}$$

and the residual yield strength f_{bT} for the reinforcing bars:

$$f_{bT}=\begin{cases}f_b & T_{max}\le 500^{o}\mathrm{C}\\ [1-5.82\times10^{-4}(T_{max}-500)]f_b & T_{max}>500^{o}\mathrm{C}\end{cases} \tag{5}$$

where E_s and f_y are the elastic modulus and yield strength of structural steel, respectively of the unexposed material, E_b and f_b are the elastic modulus and yield strength of reinforcement before fire exposure and T_{max} is the maximum temperature ever achieved during the heating and cooling phases.

The concrete compressive stress-strain relationship recommended by Han [30], which has been successfully used by Yu et al. [31] to simulate steel tube confined plain concrete stub columns, and also been used by Liu et al. [15] for finite element analysis of STCRC stub columns, is adopted in this study, and is given as follows:

$$\frac{\sigma}{f_c^{'}}=\begin{cases}2(\varepsilon/\varepsilon_0)-(\varepsilon/\varepsilon_0)^2 & \varepsilon\le\varepsilon_0\\ \dfrac{\varepsilon/\varepsilon_0}{\beta_0(\varepsilon/\varepsilon_0-1)^2+(\varepsilon/\varepsilon_0)} & \varepsilon>\varepsilon_0\end{cases} \tag{6}$$

where $\varepsilon_0=\varepsilon_c^{'}+800\xi^{0.2}\times10^{-6}$, $\varepsilon_c^{'}=(1300+12.5f_c^{'})\cdot10^{-6}$, $\beta_0=(2.36\times10^{-5})^{[0.25+(\xi-0.5)^7]}\cdot(f_c^{'})^{0.5}\cdot0.5$ and $\beta_0\ge0.12$, $\xi=f_yA_s/f_{ck}A_c$, in which A_s is the cross-sectional area of the steel tube, A_c is the cross-sectional area of the core concrete, $f_c^{'}$ is the concrete cylinder strength and f_{ck} is the characteristic concrete strength, taken as 0.67 times the concrete cube strength (f_{cu}). The initial elastic

modulus E_c was taken as $4700\sqrt{f_c^{'}}$ N/mm^2, as recommended in the ACI specification [32].

The residual properties of the concrete were determined from [33] as:

$$E_{cT} = E_c \frac{f_{cT}^{'} / \varepsilon_{cT}^{'}}{f_c^{'} / \varepsilon_c^{'}} \tag{7}$$

$$f_{cT}^{'} = \frac{f_c^{'}}{1 + 2.4(T_{max} - 20)^6 \times 10^{-17}} \tag{8}$$

$$\varepsilon_{cT}^{'} = \varepsilon_c^{'}[1 + (1500T_{max} + 5T_{max}^2) \times 10^{-6}] \tag{9}$$

For the tensile behaviour of the concrete, a linear stress-strain relationship was assumed up to the tensile strength, after which the stress was assumed to decrease linearly with increasing strain. This model was used successfully by Liu et al. [15] to simulate STCRC stub columns, and may be presented as follows:

$$\sigma = \begin{cases} E_{cT}\varepsilon & \varepsilon \le \varepsilon_{cr} \\ f_{tT}^{'}\left(\dfrac{\varepsilon - \varepsilon_{tu}}{\varepsilon_{cr} - \varepsilon_{tu}}\right) & \varepsilon_{cr} < \varepsilon \le \varepsilon_{tu} \\ 0 & \varepsilon > \varepsilon_{tu} \end{cases} \tag{10}$$

where the elastic modulus of concrete in tension is defined to be equal to that in compression, and $f_{tT}^{'} = 0.1 f_{cT}^{'}$, $\varepsilon_{cr} = \dfrac{f_{tT}^{'}}{E_{cT}}$ and $\varepsilon_{tu} = 15\varepsilon_{cr}$. The Poisson's ratios of the steel and concrete were taken as 0.3 and 0.2, respectively.

3.2.2 Temperature inputs and element meshes

The mechanical properties of the structural steel, reinforcing bars and concrete depend on the maximum temperature achieved during the heating and cooling phases. However, the maximum temperatures are not achieved simultaneously across the whole cross-section. Therefore the user subroutine USDFLD was used to extract the maximum nodal temperatures and then import them into

the stress analysis. The element meshes of the stress analysis models were kept the same as that of the corresponding heat transfer analysis model, to ensure that the thermal results can be imported correctly and efficiently, though the element type is changed from heat transfer elements to stress analysis elements. The 4-noded shell element with reduced integration (S4R) and the 8-noded solid element with reduced integration (C3D8R) were used for the steel tube and concrete, respectively; the 2-noded truss element (T3D2) was used for the reinforcing bars.

3.2.3 Initial imperfections, steel-concrete interface, and boundary conditions

Initial geometric imperfections were incorporated into the FE models in the form of the first elastic buckling mode shape with an amplitude of $L/1000$, in which L is the unsupported length of the column.

The steel tube and the core concrete were modelled separately in the FE model, and the contact algorithm in ABAQUS was used to define their interaction. The inner surface of the steel tube and the outer surface of the concrete were defined as a contact pair, of which the outer surface of the concrete was the master surface and the inner surface of the steel tube was the slave surface. "Hard contact" in the normal direction and the Coulomb friction model in the tangential direction were used to simulate the contact behaviour, with the friction coefficient and bond stress taken as 0.3 and 0.4 N/mm^2 [15], respectively, for both the unexposed and exposed members. The embedded element technique was used to specify that the reinforcing bars were embedded within the concrete.

The end plates of the columns were assumed to be elastic and were simulated with solid elements (C3D8R). Pinned boundary conditions were assigned to the end plates along one of their centrelines, and the compressive load was applied to the centre of the top end plate in the form of displacement.

The displacement controlled analysis was found to be more numerically stable than the case of load control.

3.3 Validation of the FE model

The heat transfer analysis model and the stress analysis model were validated against the tested STCRC slender columns, as shown in Fig.8 and Fig.13. The predicted temperature distributions and load versus displacement curves accord well with the tested results.

Existing tests [34] on CFST slender columns after ISO-834 standard fire were also used to validate the FE model. Details of the test specimens are listed in Table 5, in which e is the load eccentricity and a is the thickness of fire protection. The thermal conductivity, specific heat and density of the fire protection were 0.116 W/(m^{o}C), 1047 J/(kg^{o}C) and 400 ± 20 kg, respectively. The bilinear stress-strain relationship used by Han et al. [34] was also employed herein to simulate the material response of the steel tube. It should be noted that the heating phase of the CFST columns followed the ISO-834 standard fire curve, but the cooling phase was not specified, which hindered the ability to capture the maximum temperature experienced at any cross-section, which would not have occurred simultaneously. The temperature distributions corresponding to the maximum furnace temperature were therefore used to calculate the residual capacities; the same approach was followed in [34]. The predicted and tested axial load versus lateral displacement curves, together with original authors' predictions, are presented in Fig.14, confirming that the FE model can also be used to predict behaviour of CFST slender columns after fire exposure.

4. Parametric studies and design method

4.1 Parametric studies

Having validated the FE models, parametric studies were performed to extend the ranges of the key investigated parameters, and to analyse their influence on the residual capacity of STCRC slender columns following fire exposure. The considered key parameters were exposure time, cross-section diameter, slenderness ratio, compressive strength of concrete, yield strength of steel tube, yield strength of reinforcing bars, steel tube to concrete area ratio and reinforcement ratio. The values of these parameters are given in Table 6.

The influences of these parameters on the residual capacity of STCRC slender columns are shown in Fig.15. It can be seen that the residual capacities decrease as the heating time increases, and increase as the cross-section diameter becomes larger. Clearly, with increasing heating time, the deterioration of material intensifies, resulting in a reduction of residual capacity. Conversely, as the cross-section diameter increases, the deterioration of material reduces due to the lower temperature levels attained; in addition to the straightforward increase in cross-sectional area, this also contributes to the increase of residual capacity. The residual capacity decreases approximately linearly with increasing slenderness ratio, and increases approximately linearly with increasing material strengths, steel tube to concrete area ratio and reinforcement ratio.

4.2 Design method

The load bearing capacities of slender columns can be expressed as follows:

$$N_{\mathrm{e}} = \chi N_{\mathrm{u}} \tag{11}$$

where N_{e} is the load-bearing capacity of the column, χ is the buckling reduction factor and N_{u} is the

cross-sectional capacity of the column, which can be calculated based on the proposal of Liu and Zhou [11]. The results of the parametric study, showing the influences of the key variables on the buckling reduction factor, are presented in Fig.16. As expected, the slenderness ratio has a significant influence on the buckling reduction factor, whereas the heating time and cross-section diameter have some effect and other factors have negligible influence.

Based on the above studies, and considering first the buckling behaviour of STCRC slender columns not exposed to fire, the following buckling reduction factor is proposed:

$$\chi = 1.0 - 0.005\lambda \tag{12}$$

where λ is the slenderness ratio of the column defined by Eq.(1).

Comparisons of the predicted capacities with the FE and test results are shown in Fig.17, where the accuracy of the design method is illustrated.

For STCRC slender columns after fire exposure, it is proposed to incorporate the influence of temperature into the buckling reduction factor as follows:

$$\chi_{\mathbf{T}} = 1.0 - 0.005(\lambda + \frac{2t_{\mathbf{h}}}{D}) \tag{13}$$

where t_h is the heating time, following the standard fire curve, in hours and D is the cross-section diameter in metres. Note that Eq.(13) simplifies to Eq.(12) when t_h=0.

The cross-sectional capacity of STCRC columns after fire exposure can be predicted with the design method proposed by Liu et al. [15], which is given as follows:

$$N_{uT} = \overline{f}_{ccT} A_c + f_{bT} A_b \tag{14}$$

where

$$f_{bT} = \begin{cases} f_b & t_h \le 1.0 \\ (1.075 - 0.075 t_h) f_b & 1.0 < t_h \le 3.0 \end{cases} \tag{15}$$

$$\overline{f}_{\mathrm{ccT}}=\left(-1.254+2.254\sqrt{1+7.94\frac{f_{\mathrm{rT}}}{\overline{f}'_{\mathrm{cT}}}}-2\frac{f_{\mathrm{rT}}}{\overline{f}'_{\mathrm{cT}}}\right)\overline{f}'_{\mathrm{cT}} \tag{16}$$

$$\overline{f}'_{\mathrm{cT}}=k\times[1-(\frac{0.066}{D}-0.008)t_{\mathrm{h}}]f'_{\mathrm{c}} \tag{17}$$

$$f_{\mathrm{rT}}=\frac{2t_{\mathrm{s}}f_{\mathrm{yT}}}{D-2t_{\mathrm{s}}} \tag{18}$$

$$f_{\mathrm{yT}}=(0.02t_{\mathrm{h}}^2-0.15t_{\mathrm{h}}+1.0)f_y \tag{19}$$

where A_{c} and A_{b} are cross-sectional area of the concrete and reinforcement, respectively, f_{b} and f_{bT} are the yield strength of reinforcement before and post fire exposure, $\overline{f}_{\mathrm{ccT}}$ and $\overline{f}'_{\mathrm{cT}}$ are the equivalent residual compressive strength of confined concrete and unconfined concrete, respectively, f_{y} and f_{yT} are the yield strength of the steel tube before and post fire exposure, f_{rT} is the confining stress provided by the steel tube to the concrete, t_{h} is the heating time in hours, D is the cross-sectional diameter in metres, t_{s} is the thickness of the steel tube in metres and k is a parameter accounting for the effect of the delay in temperature rise through the cross-section, taken as 1.0 and 0.98 for the unexposed and exposed conditions, respectively.

The load-bearing capacity of STCRC slender columns after fire exposure, N_{eT}, can be predicted by substituting χ_{T} and N_{uT} into Eq.(11). Comparisons of the predicted residual capacities with the FE and test results are presented in Fig.18, good agreement may be seen.

The limits of validity of the above design method are: D =0.2 – 1.5 m, t_{h}=0 – 3 h, λ=20 – 60, f_{c}'=20 N/mm^2 - 50 N/mm^2, f_{y}=235 N/mm^2 - 420 N/mm^2, f_{b}=335 N/mm^2 - 500 N/mm^2, α_{s}=2% - 4%, and α_{b}=2% - 6%.

5. Conclusions

Experimental and numerical studies were carried out to investigate the post-fire behaviour of slender

reinforced concrete columns confined by circular steel tubes. Fourteen specimens were tested after exposure to the ISO-834 standard fire, to study their fundamental behaviour and to generate data for validation of FE models. A sequentially coupled thermal-stress analysis model was developed with the program ABAQUS to study the influence of some key parameters on the residual capacity. A simplified design method was then proposed for evaluating residual capacities of STCRC slender columns, after ISO-834 standard fire exposure. Based on the described studies, the following conclusions can be drawn:

(1) The maximum temperature achieved during the heating and cooling phases of the examined STCRC slender columns was not uniform across the cross-section, and decreased from the outer steel tube to the concrete centre. Meanwhile, the maximum temperatures were also not achieved simultaneously across the section, due to the high thermal capacity of concrete and the protection of surrounding materials.

(2) The failure mode of the examined STCRC slender columns was characterised by global bucking, accompanied by local buckling in some cases. Although compressive crushing occurred in the concrete, the concrete core remained intact due to the confinement of the outer steel tube.

(3) The residual capacities of the investigated STCRC slender columns were found to be sensitive to the heating time, cross-sectional dimension, slenderness ratio, material strength, steel tube to concrete area ratio and reinforcement ratio, whereas the buckling reduction factor was seen to depend primarily on the slenderness ratio, heating time and cross-sectional dimension.

(4) A simplified design method was proposed for predicting the residual capacity of STCRC slender columns after ISO-834 standard fire exposure, and may be used to provide a preliminary assessment

of the residual capacity after fire exposure.

6. Acknowledgement

The research presented in this paper was sponsored by the National Natural Science Foundation (NO. 51278153), a Special Fund of Harbin Technological Innovation (NO. 2012RFLXG025) and the China Scholarship Council (CSC); their financial support is highly appreciated.

7. References

[1] Gardner NJ, Jacobson ER. Structural behavior of concrete filled steel tubes. ACI Journal Proceedings 1967; 64(7): 404-13.

[2] Orito Y, Sato T, Tanaka N, Watanabe Y. Study on the unbonded steel tube concrete structure. In : Composite Construction in Steel and Concrete, ASCE 1987; 786-804.

[3] Prion HGL, Boehme J. Beam-column behavior of steel tubes filled with high strength concrete. Canadian Journal of Civil Engineering 1994; 21: 207-18.

[4] O'Shea MD, Bridge RQ. Tests on circular thin-walled steel tubes filled with medium and high strength concrete. University of Sydney, Department of Civil Engineering, Centre for Advanced Structural Engineering Research Report No. 754; 1997.

[5] O'Shea MD, Bridge RQ. Tests on circular thin-walled steel tubes filled with very high strength concrete. University of Sydney, Department of Civil Engineering, Centre for Advanced Structural Engineering Research Report No. 755; 1997.

[6] Fam A, Qie FS, Rizkalla S. Concrete-filled steel tubes subjected to axial compression and lateral cyclic loads. Journal of Structural Engineering, ASCE 2004; 130(4): 631-40.

[7] Tomii M, Sakino K, Watanabe K, Xiao Y. Lateral Load Capacity of Reinforced Concrete Short Columns Confined by Steel Tube. In: Proceedings of the International Speciality Conference on Concrete Filled Steel Tubular Structures, Harbin, China, 1985; 19-26.

[8] Tomii M, Sakino K, Xiao Y, Watanabe K. Earthquake Resisting Hysteretic Behavior of

Reinforced Concrete Short Columns Confined by Steel Tube. In: Proceedings of the International Speciality Conference on Concrete Filled Steel Tubular Structures, Harbin, China, 1985; 119-25.

[9] Sakino K, Tomii M, Watanabe K. Sustaining Load Capacity of Plain Concrete Stub Columns Confined by Circular Steel Tube. In: Proceeding of the International Speciality Conference on Concrete Filled Steel Tubular Structures, Harbin, China, 1985; 112-8.

[10] Yu Q, Tao Z, Liu W, Chen ZB. Analysis and calculations of steel tube confined concrete (STCC) stub columns. Journal of Constructional Steel Research 2010; 66: 53-64.

[11] Liu JP, Zhou XH. Behavior and strength of tubed RC stub columns under axial compression. Journal of Constructional Steel Research 2010; 66: 28-36.

[12] Aboutaha RS, Machado R. Seismic resistance of steel confined reinforced concrete SCRC columns. The Structural Design of Tall Buildings 1998; 7(3): 251-60.

[13] Zhou XH, Liu JP. Seismic behavior and shear strength of tubed RC short columns. Journal of Constructional Steel Research 2010; 66: 385-97.

[14] Han LH, Qu H, Tao Z, Wang ZF. Experimental behaviour of thin-walled steel tube confined concrete column to RC beam joints under cyclic loading. Thin-walled Structures 2009; 47: 847-57.

[15] Liu FQ, Gardner L, Yang H. Post-fire behaviour of reinforced concrete stub columns confined by circular steel tubes. Journal of Constructional Steel Research (submitted).

[16] ISO-834. Fire resistance tests - elements of building construction. Switzerland: International Organization for Standardization; 1975.

[17] GB/T 228-2010. Metallic materials-Tensile testing-Part 1: Method of test at room temperature. Beijing: China Standard Press; 2010 [in Chinese].

[18] Abrams MS. Compressive strength of concrete at temperatures to 1600 F. ACI Special Publication 1971; 25: 33-58.

[19] Phan LT, Carino NJ. Review of mechanical properties of HSC at elevated temperature. Journal

of materials in Civil Engineering, ASCE 1998; 10(1): 58-64.

[20] Hertz KD. Concrete strength for fire safety design. Magazine of Concrete Research 2005; 57(8): 445-53.

[21] Huo JS, Huang GW, Xiao Y. Effects of sustained axial load and cooling phase on post-fire behaviour of concrete-filled steel tubular stub columns. Journal of Constructional Steel Research 2009; 65: 1664-76.

[22] Tao J, Yuan Y, Taerwe L. Compressive strength of self-compacting concrete during high-temperature exposure. Journal of Materials in Civil Engineering, ASCE 2010; 22(10): 1005-11.

[23] Huo JS, Zeng X, Xiao Y. Cyclic behaviours of concrete-filled steel tubular columns with pre-load after exposure to fire. Journal of Constructional Steel Research 2011; 67: 727-39.

[24] Ding J, Wang YC. Realistic modelling of thermal and structural behaviour of unprotected concrete filled tubular columns in fire. Journal of Constructional Steel Research 2008; 64: 1086-102.

[25] Lu H, Zhao XL, Han LH. FE modelling and fire resistance design of concrete filled double skin tubular columns. Journal of Constructional Steel Research 2011; 67(11): 1733-48.

[26] Lv XT, Yang H, Zhang SM. Effect of contact thermal resistance on temperature distributions of concrete-filled steel tubes in fire. Journal of Harbin Institute of Technology 2011; 18(1): 81-8.

[27] Lie TT. Fire resistance of circular steel columns filled with bar-reinforced Concrete. Journal of Structural Engineering, ASCE 1994; 120(5): 1489-509.

[28] Lu H, Zhao XL, Han LH. Finite element analysis of temperatures in concrete filled double skin steel tubes exposed to fires. In: 4th International structural engineering and construction conference, Melbourne , Australia , 2007; 1151-6.

[29] Tao Z, Wang XQ, Uy B. Stress-strain curves of structural steel and reinforcing steel after exposure to elevated temperatures. Journal of Materials in Civil Engineering, ASCE 2013; 25(9): 1306-16.

[30] Han LH, Yao GH, Tao Z. Performance of concrete-filled thin-walled steel tubes under pure torsion. Thin-Walled Structures 2007; 45(1): 24-36.

[31] Yu Q, Tao Z, Liu W, Chen ZB. Analysis and calculations of steel tube confined concrete (STCC) stub columns. Journal of Constructional Steel Research 2010; 66(1): 53-64.

[32] ACI 318M-08. Building code requirements for structural concrete and Commentary. USA: American Concrete Institute; 2008.

[33] Li W, Guo ZH. Experimental investigation of strength and deformation of concrete at elevated temperatures. Chinese Journal on Building Structures 1993; 14(1): 8-16 [in Chinese].

[34] Han LH, Huo JS. Concrete-filled hollow structural steel columns after exposure to ISO-834 fire standard. Journal of Structural Engineering, ASCE 2003; 129(1): 68-78.

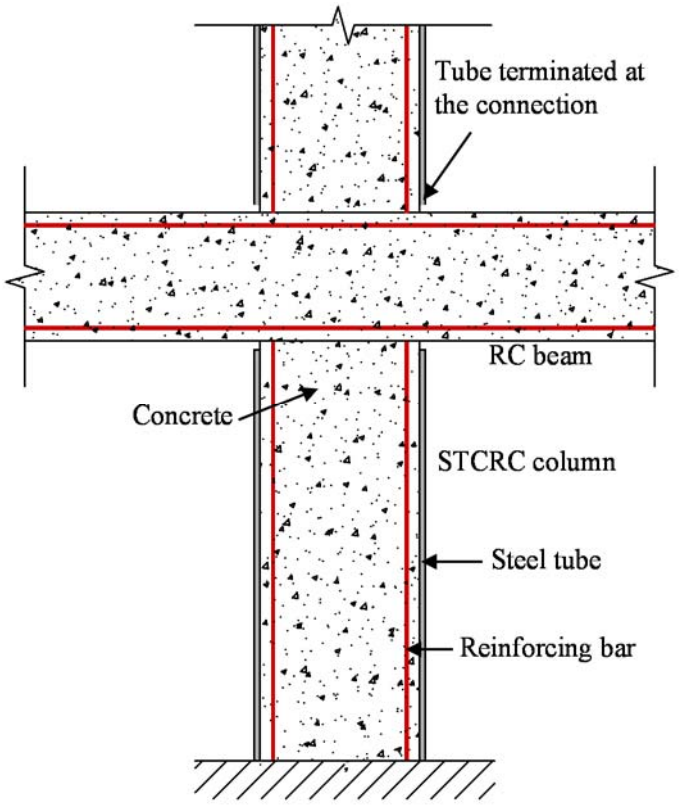

Fig.1 Schematic view of the STCRC column and its beam to column connection.

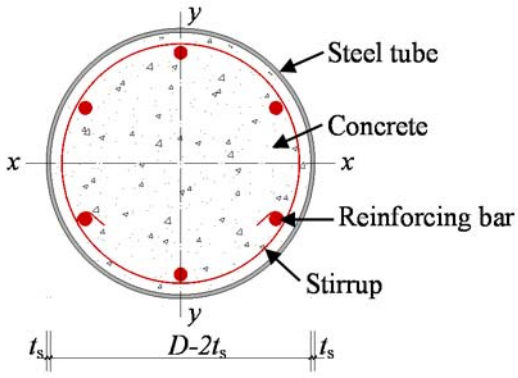

Fig.2 Typical cross-section of specimens

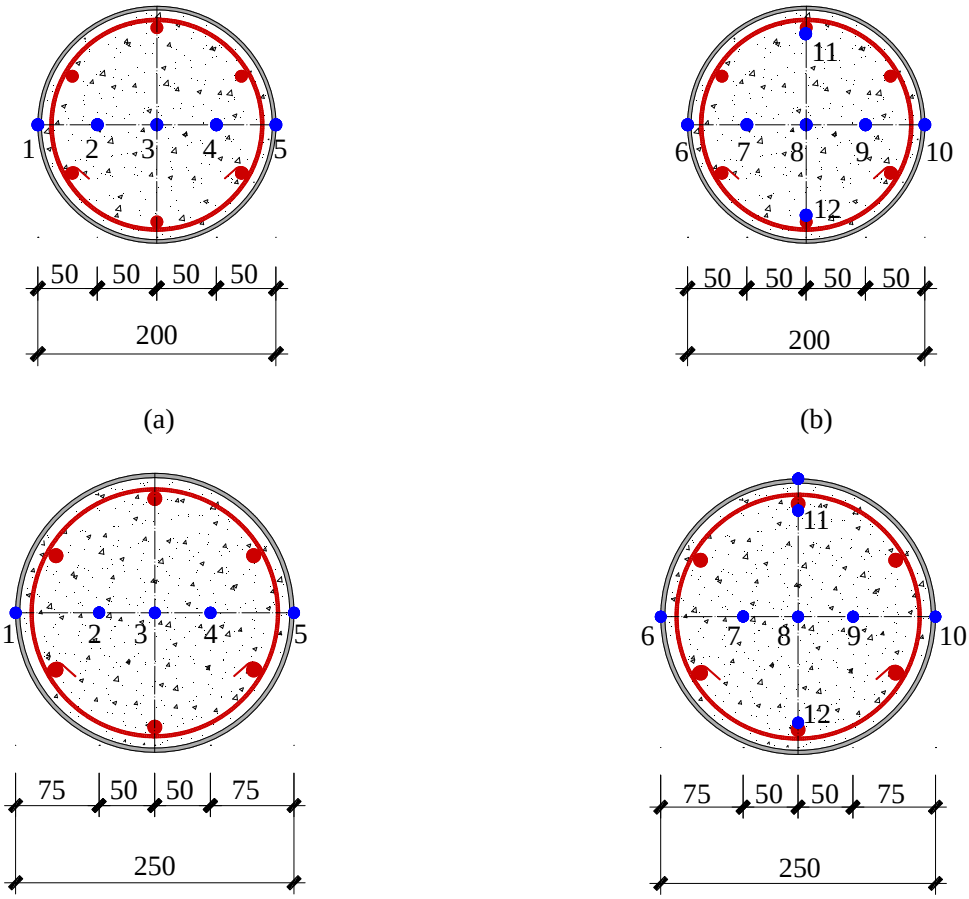

Fig.3 Layouts of thermocouples: C200-30min: (a) top; (b) bottom; C250-30min and C250-60min: (c) top; and (d) bottom (unit: mm).

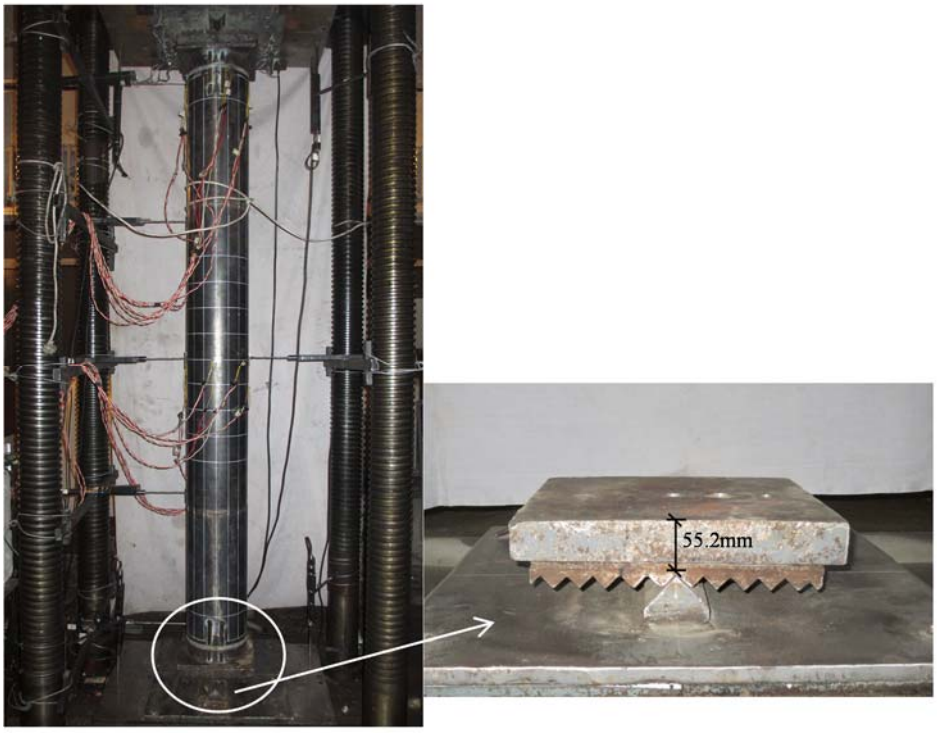

Fig.4 Typical test setup for the STCRC slender columns

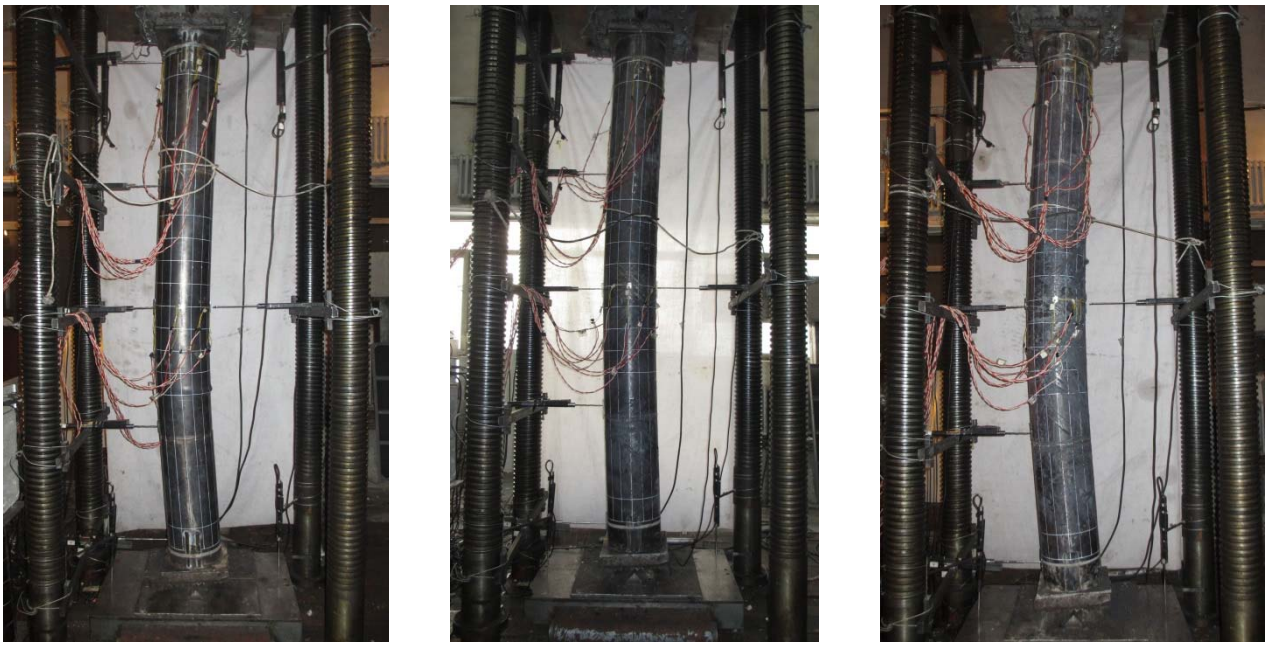

(a) (b) (c)

Fig.5 Typical failure modes of STCRC slender columns: (a) C250-10-30-0, t_h=0min; (b) C250-10-30-30, t_h=30min; and (c) C250-10-30-60, t_h=60min.

(a) (b) (c)

Fig.6 Failed specimens upon removal of outer steel tubes: (a) C250-10-30-0, t_h=0min; (b) C250-10-30-30, t_h=30min; and (c) C250-10-30-60, t_h=60min.

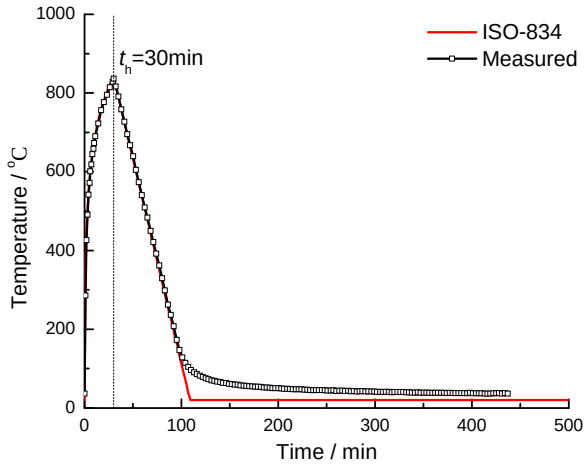

(a)

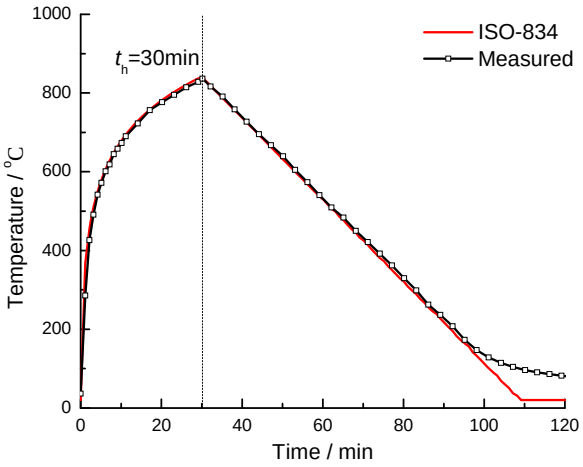

(b)

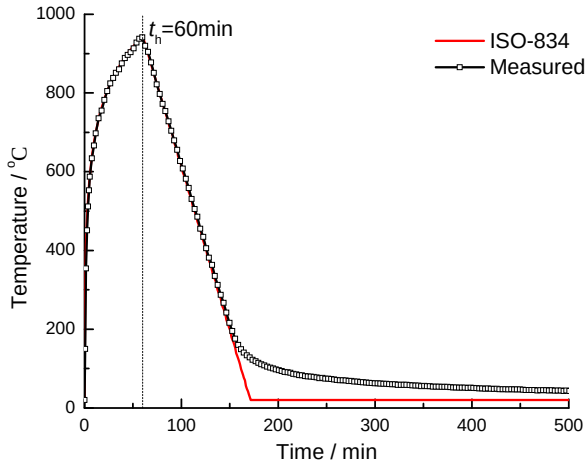

(c)

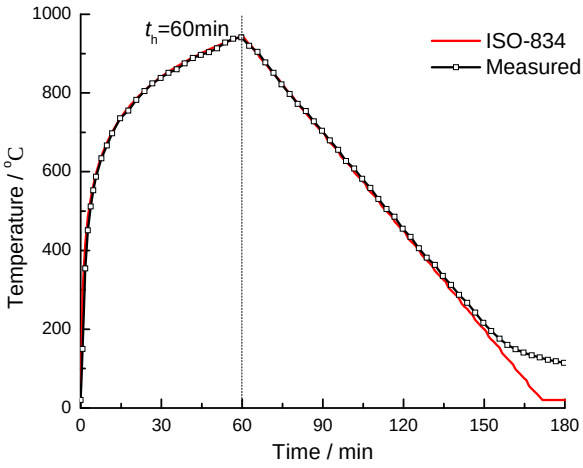

(d)

Fig.7 Comparisons of measured furnace temperatures with ISO-834 standard fire curve: (a) 30min; (b) enlargement of partial portion of (a); (c) 60min; and (d) enlargement of partial portion of (c).

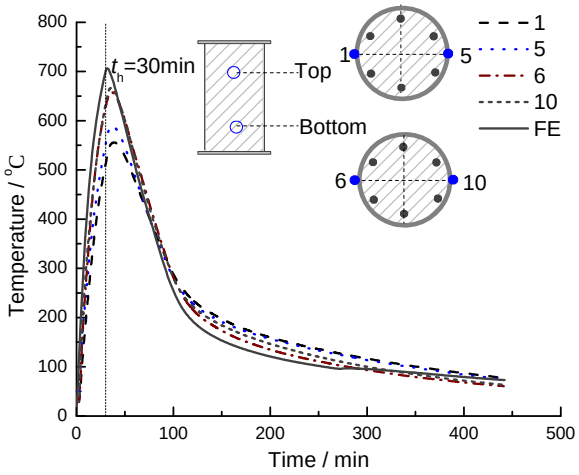
Temperature / °C
Time / min
t_h=30min
Top
Bottom
1
5
6
10
FE

(a)

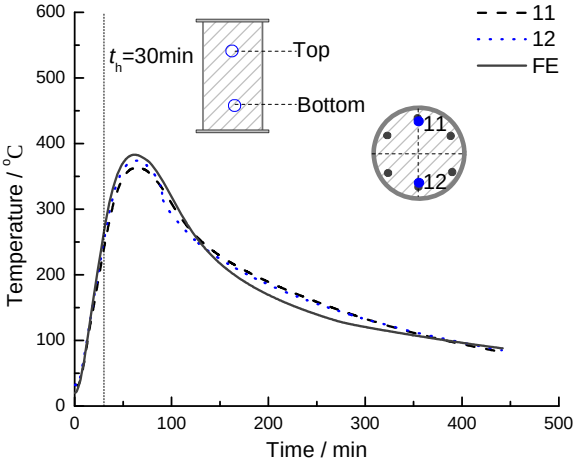
Temperature / °C
Time / min
t_h=30min
Top
Bottom
11
12
FE

(b)

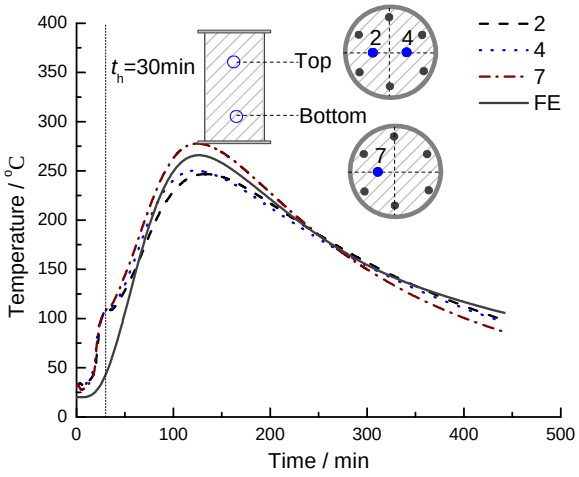
Temperature / °C
Time / min
t_h=30min
Top
Bottom
2
4
7
FE

(c)

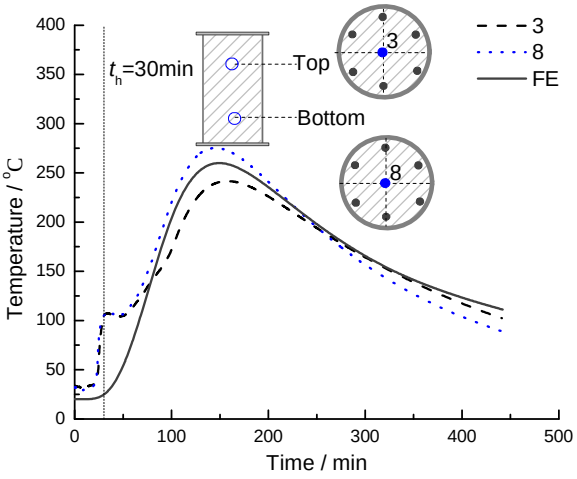
Temperature / °C
Time / min
t_h=30min
Top
Bottom
3
8
FE

(d)

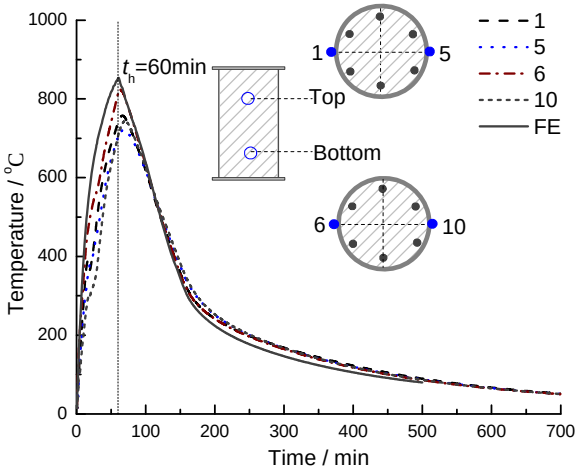
Temperature / °C
Time / min
t_h=60min
Top
Bottom
1
5
6
10
FE

(e)

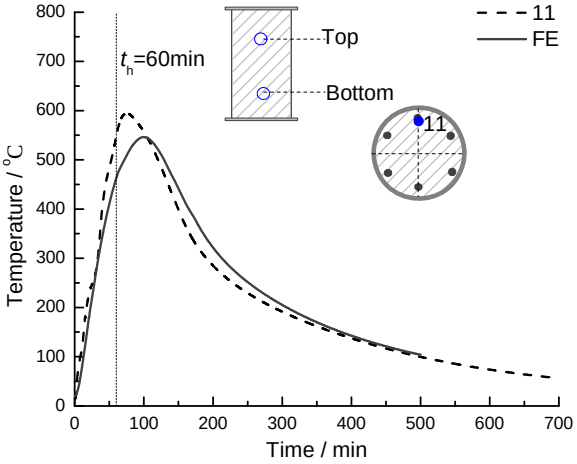
Temperature / °C
Time / min
t_h=60min
Top
Bottom
11
FE

(f)

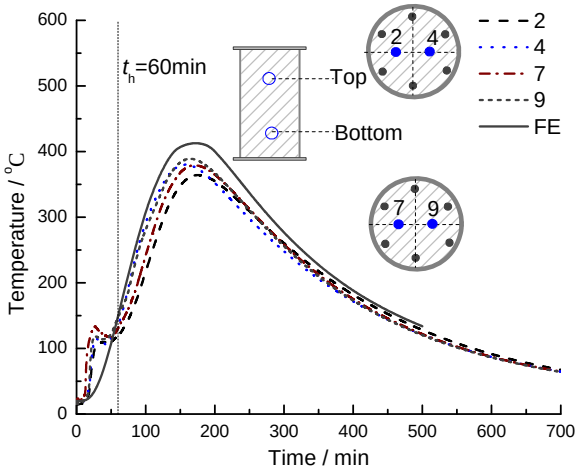

(g)

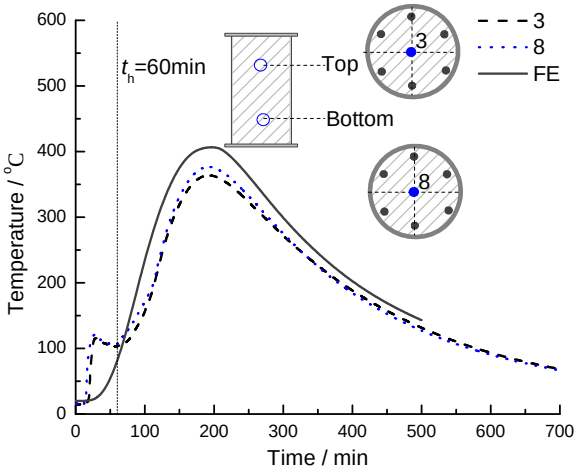

(h)

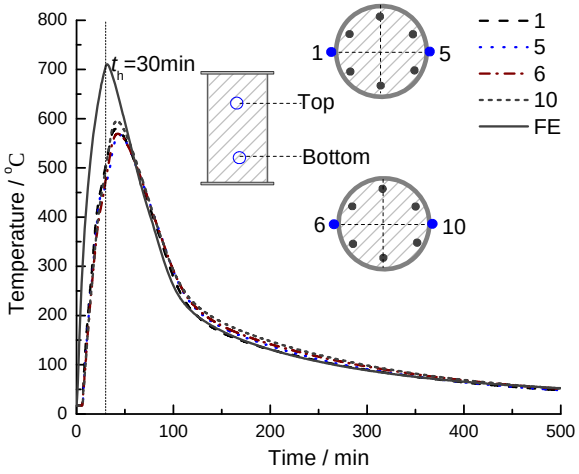

(i)

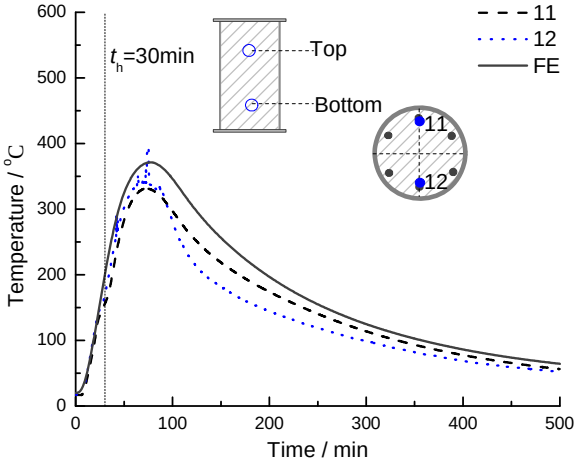

(j)

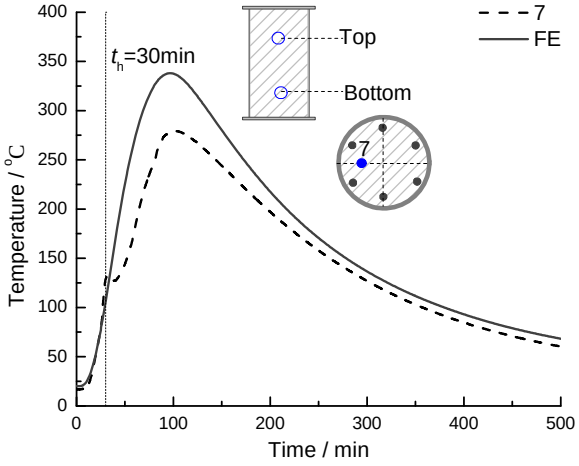

(k)

Fig.8 Measured and predicted cross-sectional temperatures of specimens: C250-30min: (a) steel tube; (b) reinforcement bars; (c) and (d) concrete; C250-60min: (e) steel tube; (f) reinforcement bars; (g) and (h) concrete; and C200-30min: (i) steel tube; (j) reinforcement bars; (k) concrete.

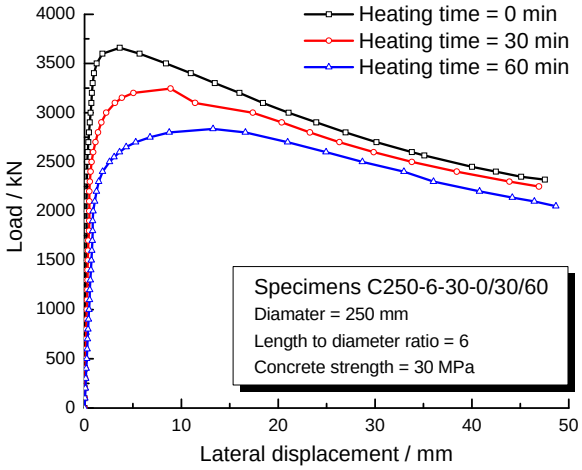

(a)

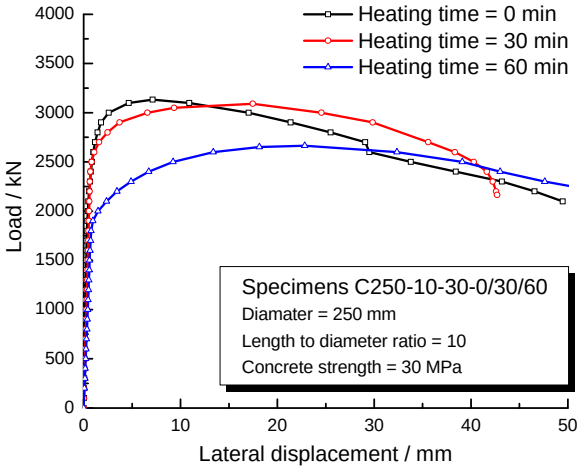

(b)

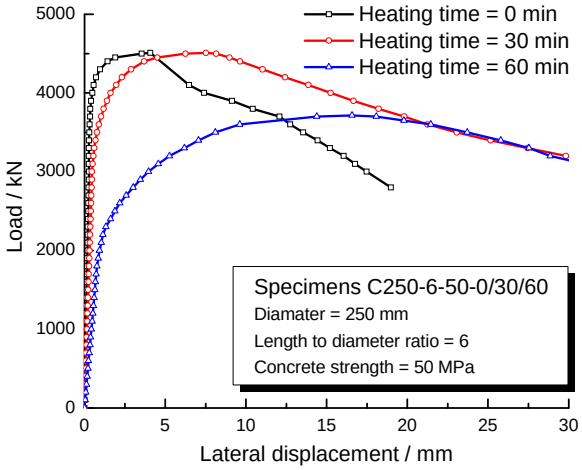

(c)

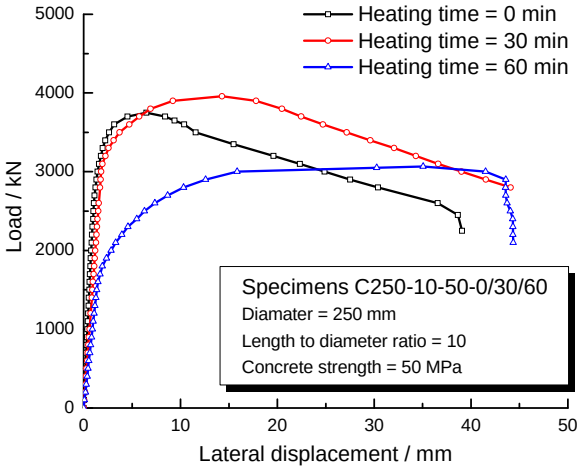

(d)

Fig.9 Influence of exposure time on load-lateral displacement curves: (a) C250-6-30-0/30/60; (b) C250-10-30-0/30/60; (c) C250-6-50-0/30/60; and (d) C250-10-50-0/30/60.

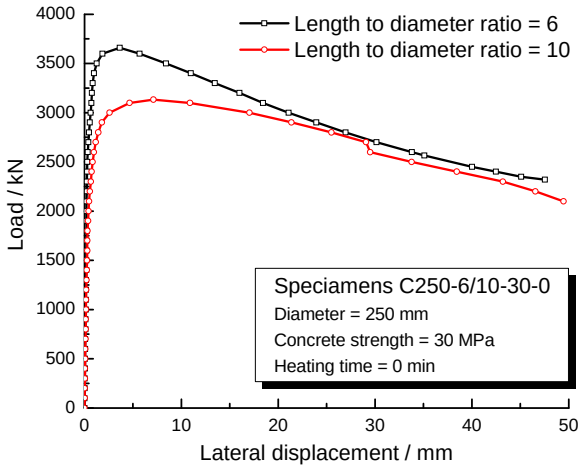
Length to diameter ratio = 6
Length to diameter ratio = 10
Speciamens C250-6/10-30-0
Diameter = 250 mm
Concrete strength = 30 MPa
Heating time = 0 min
Load / kN
Lateral displacement / mm

(a)

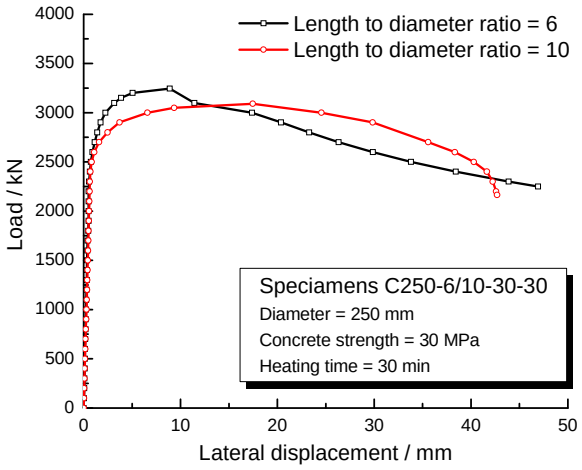
Length to diameter ratio = 6
Length to diameter ratio = 10
Speciamens C250-6/10-30-30
Diameter = 250 mm
Concrete strength = 30 MPa
Heating time = 30 min
Load / kN
Lateral displacement / mm

(b)

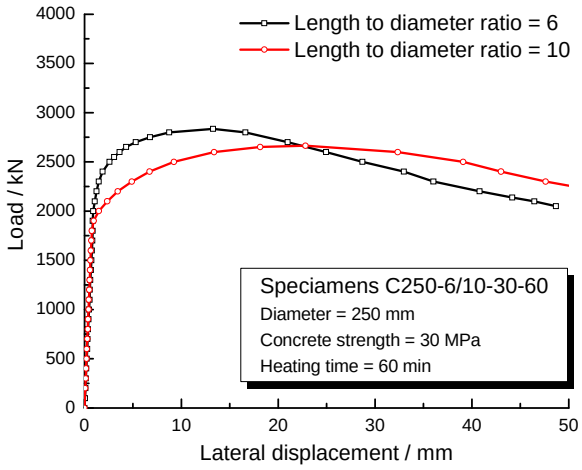
Length to diameter ratio = 6
Length to diameter ratio = 10
Speciamens C250-6/10-30-60
Diameter = 250 mm
Concrete strength = 30 MPa
Heating time = 60 min
Load / kN
Lateral displacement / mm

(c)

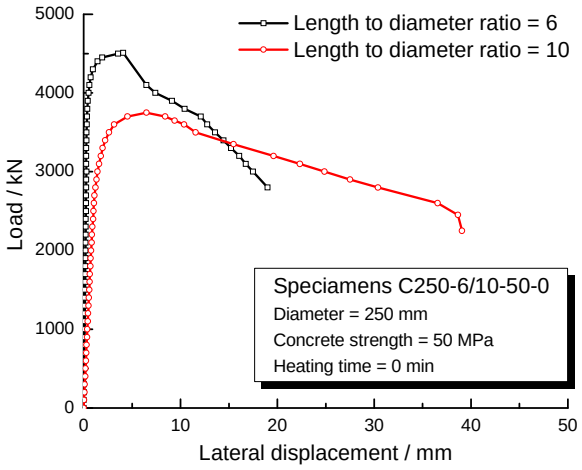
Length to diameter ratio = 6
Length to diameter ratio = 10
Speciamens C250-6/10-50-0
Diameter = 250 mm
Concrete strength = 50 MPa
Heating time = 0 min
Load / kN
Lateral displacement / mm

(d)

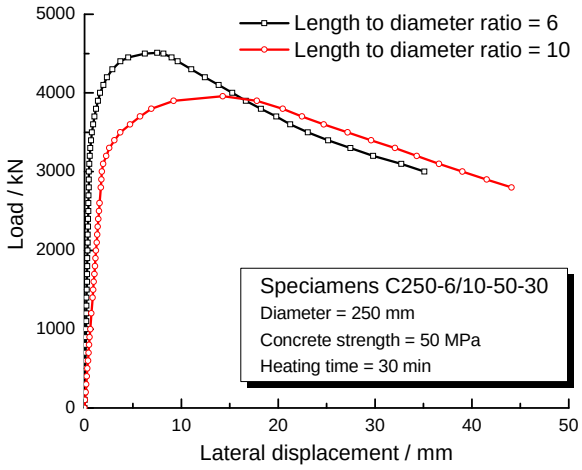
Length to diameter ratio = 6
Length to diameter ratio = 10
Speciamens C250-6/10-50-30
Diameter = 250 mm
Concrete strength = 50 MPa
Heating time = 30 min
Load / kN
Lateral displacement / mm

(e)

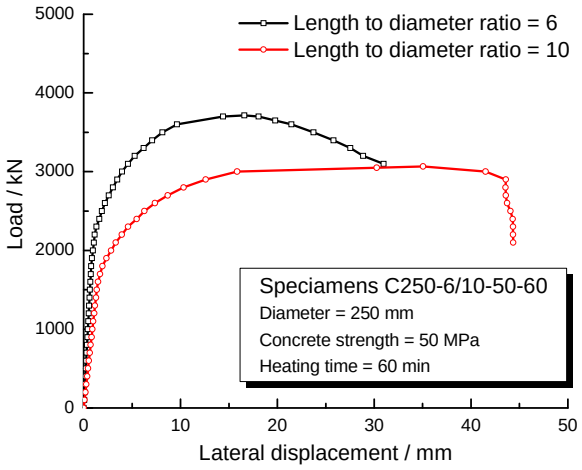
Length to diameter ratio = 6
Length to diameter ratio = 10
Speciamens C250-6/10-50-60
Diameter = 250 mm
Concrete strength = 50 MPa
Heating time = 60 min
Load / kN
Lateral displacement / mm

(f)

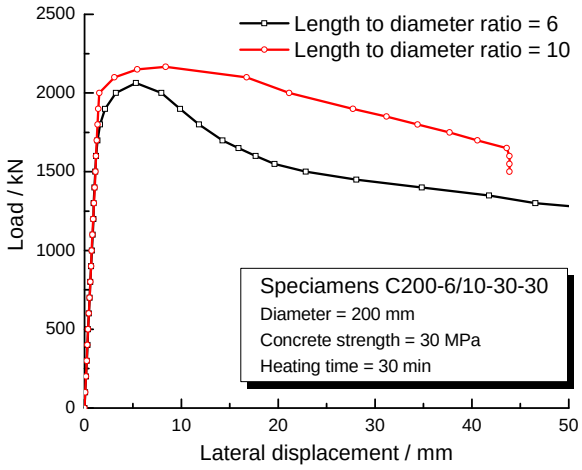

(g)

Fig.10 Influence of slenderness on load-lateral displacement curves: (a) C250-6/10-30-0; (b) C250-6/10-30-30; (c) C250-6/10-30-60; (d) C250-6/10-50-0; (e) C250-6/10-50-30; (f) C250-6/10-50-60; and (g) C200-6/10-30-30.

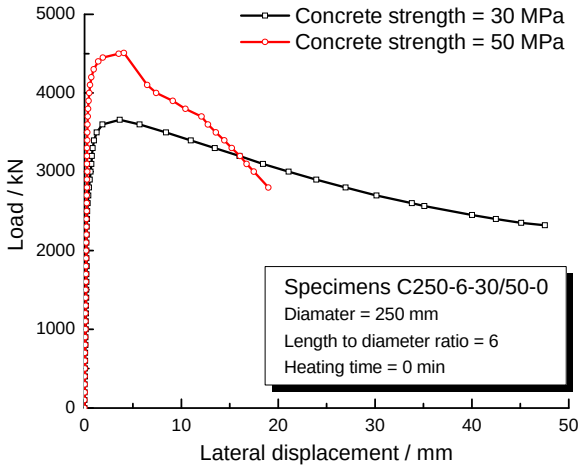

(a)

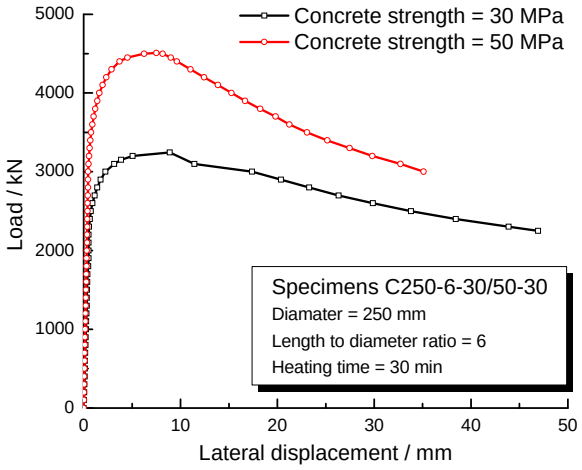

(b)

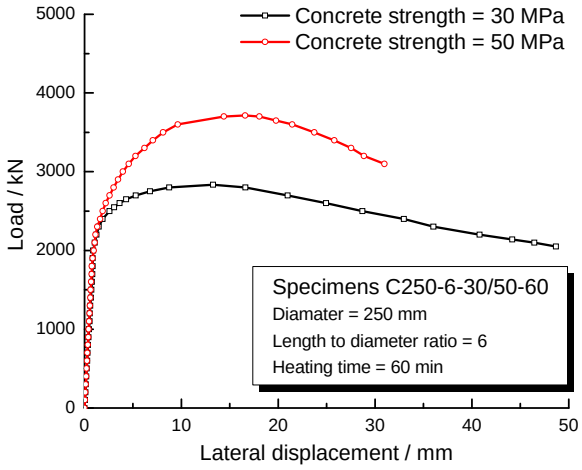

(c)

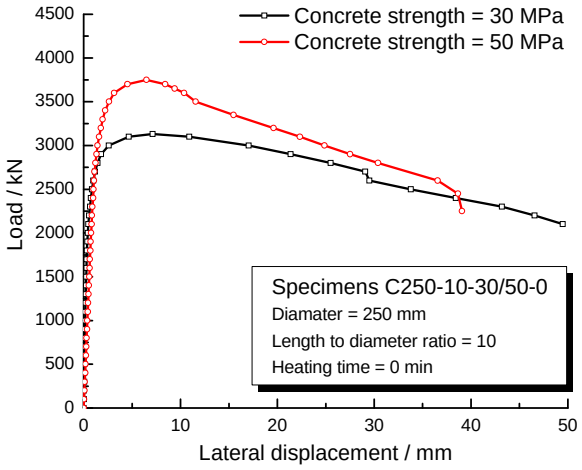

(d)

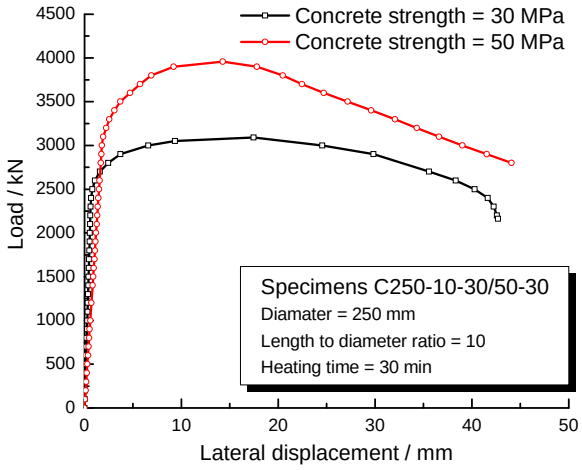

(e)

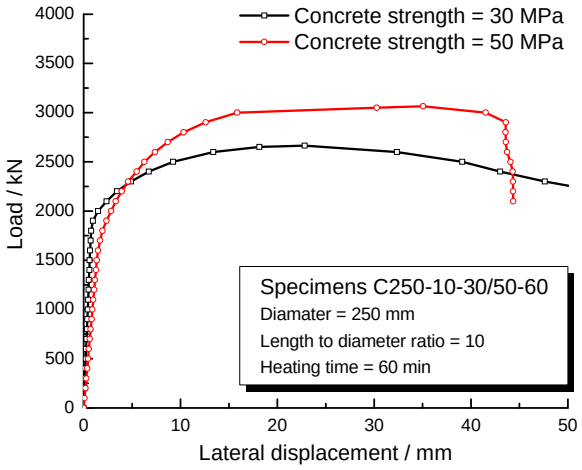

(f)

Fig.11 Influence of concrete strength on load-lateral displacement curves: (a) C250-6-30/50-0; (b) C250-6-30/50-30; (c) C250-6-30/50-60; (d) C250-10-30/50-0; (e) C250-10-30/50-30; and (f) C250-10-30/50-60.

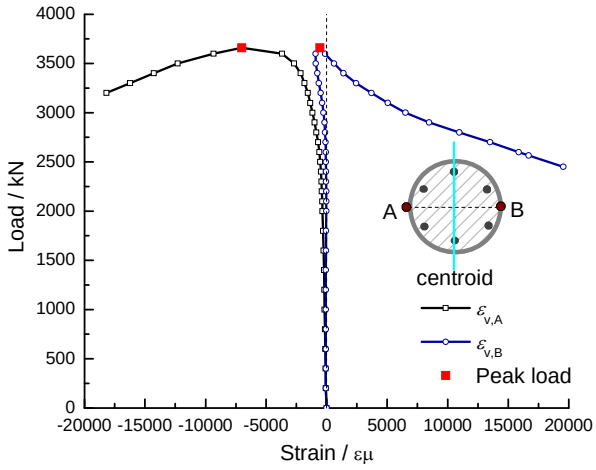

(a)

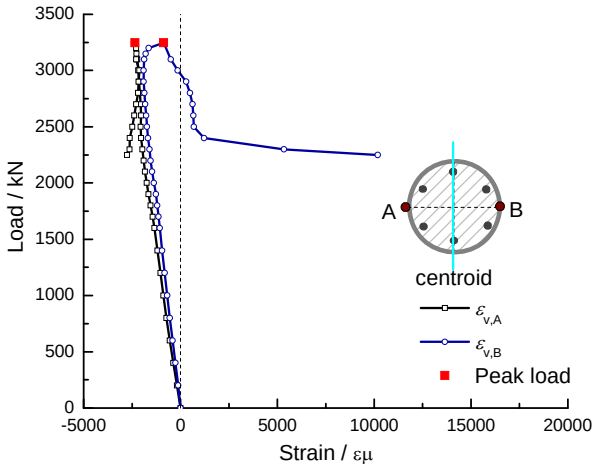

(b)

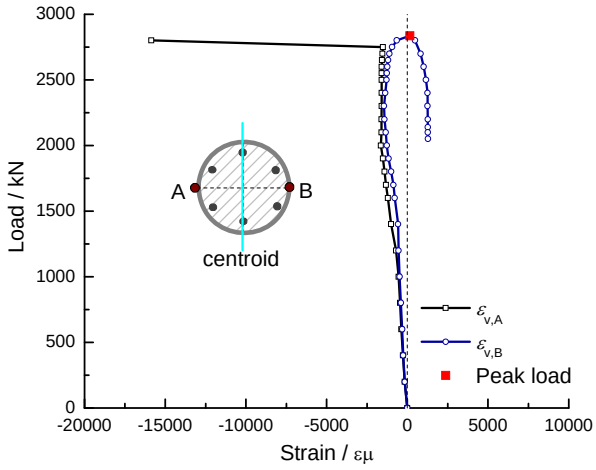

(c)

Fig.12 Development of longitudinal strains in steel tube: (a) C250-6-30-0; (b) C250-6-30-30; and (c) C250-6-30-60.

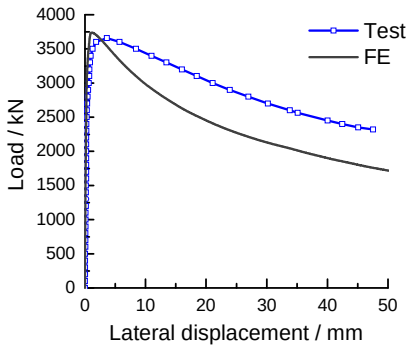

(a)

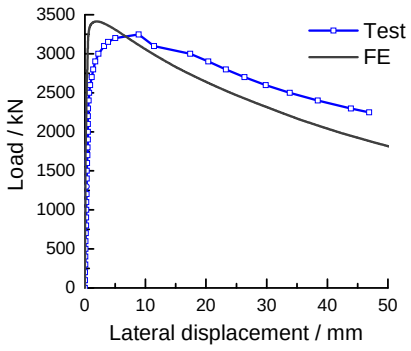

(b)

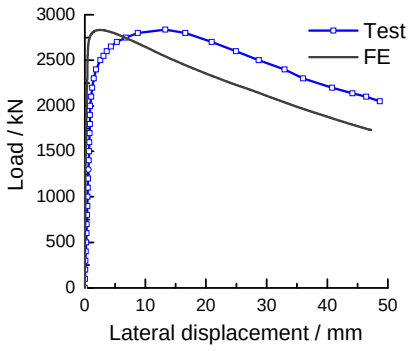

(c)

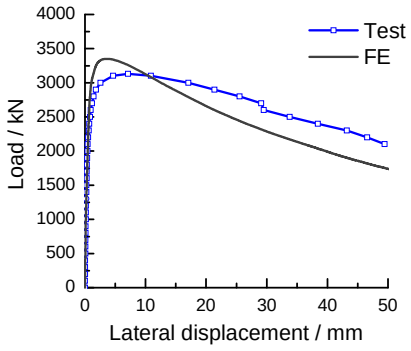

(d)

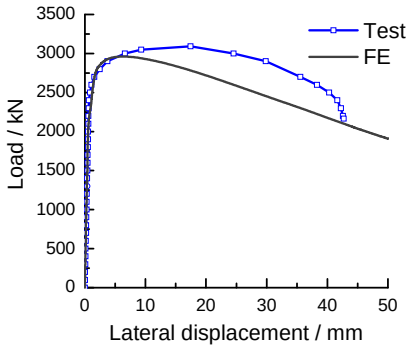

(e)

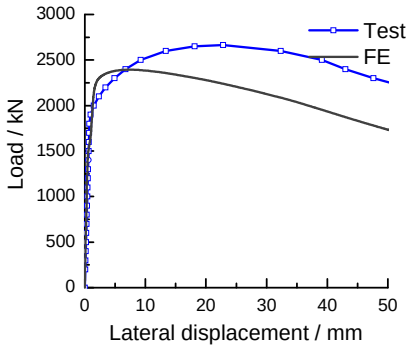

(f)

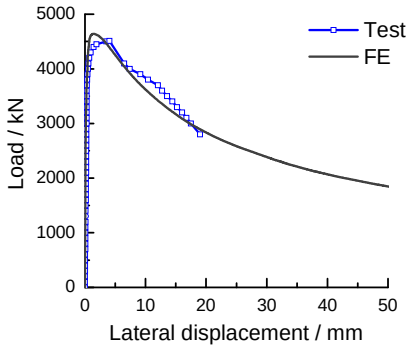

(g)

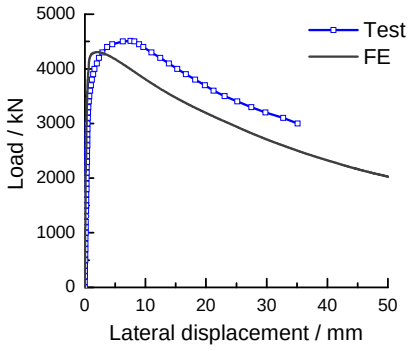

(h)

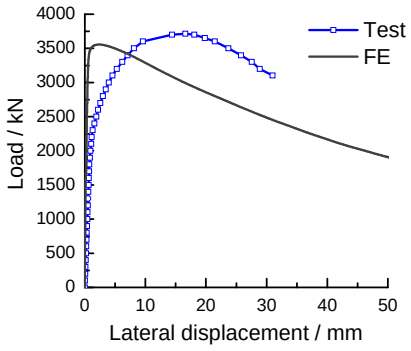

(i)

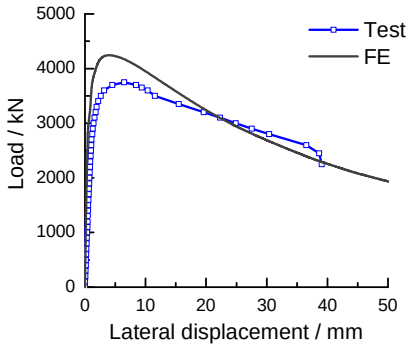

(j)

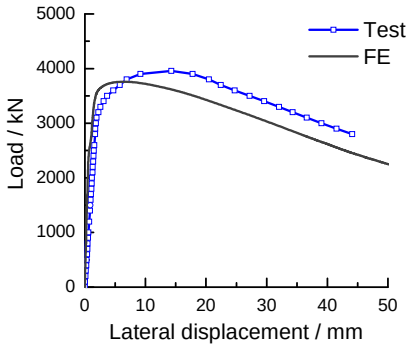

(k)

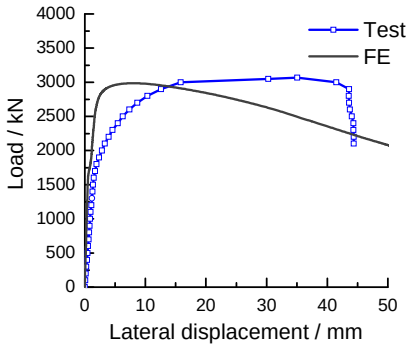

(m)

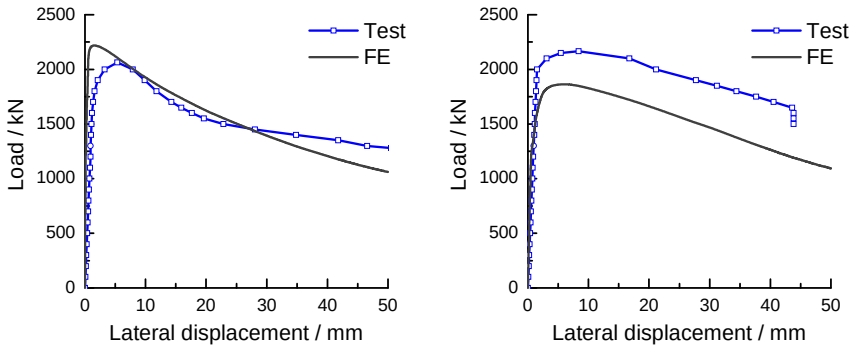

(n) (o)

Fig.13 Comparisons between predicted and tested load-lateral displacement curves of STCRC slender columns: (a) C250-6-30-0; (b) C250-6-30-30; (c) C250-6-30-60; (d) C250-10-30-0; (e) C250-10-30-30; (f) C250-10-30-60; (g) C250-6-50-0; (h) C250-6-50-30; (i) C250-6-50-60; (j) C250-10-50-0; (k) C250-10-50-30; (m) C250-10-50-60; (n) C200-6-30-30; and (o) C200-10-30-30.

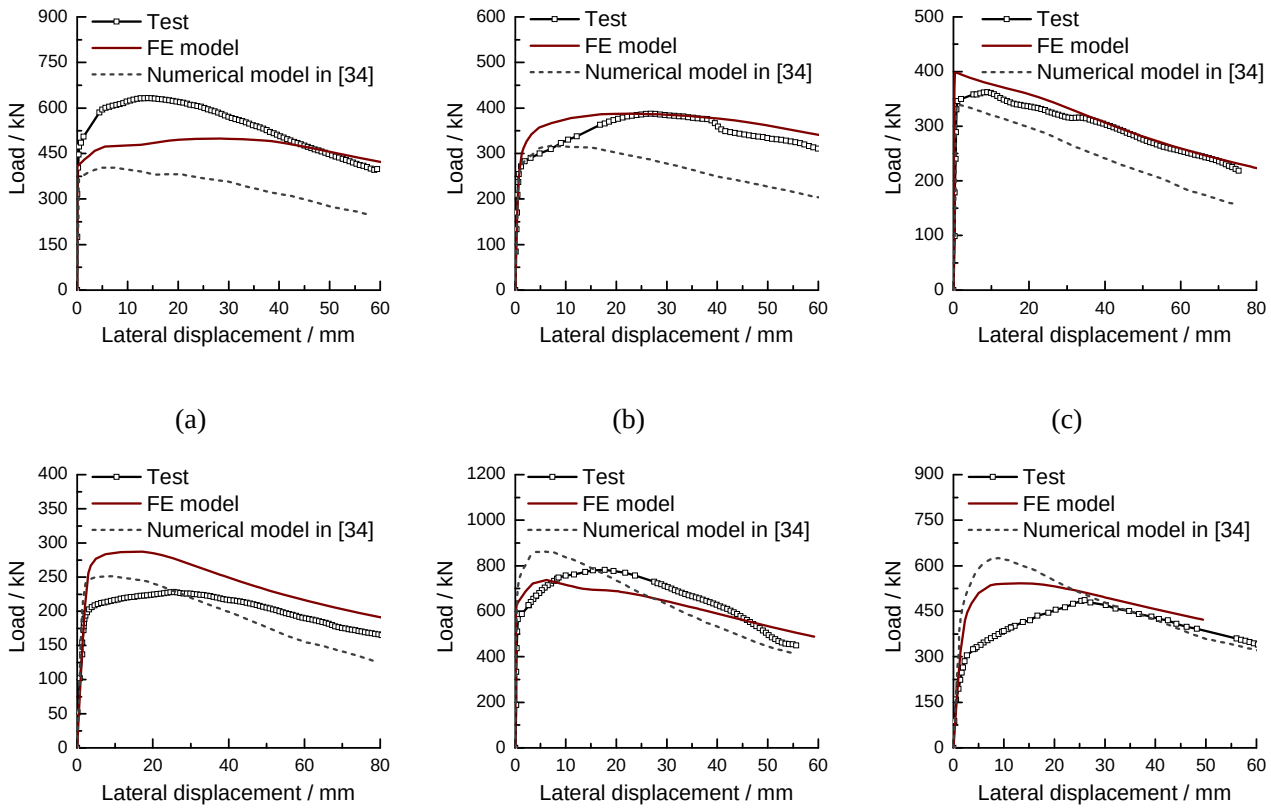

Fig.14 Comparisons between predicted and tested load-lateral displacement curves of CFST slender columns [34]: (a) C1; (b) C2; (c) C3; (d) C4; (e) CP1; and (f) CP2.

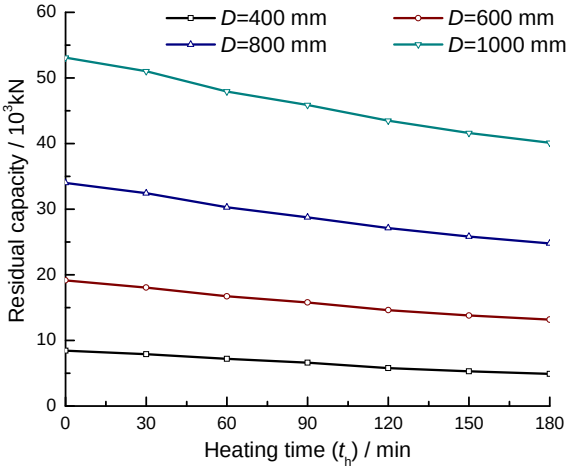
D=400 mm
D=600 mm
D=800 mm
D=1000 mm
Residual capacity / 10^3kN
Heating time (t_h) / min

(a)

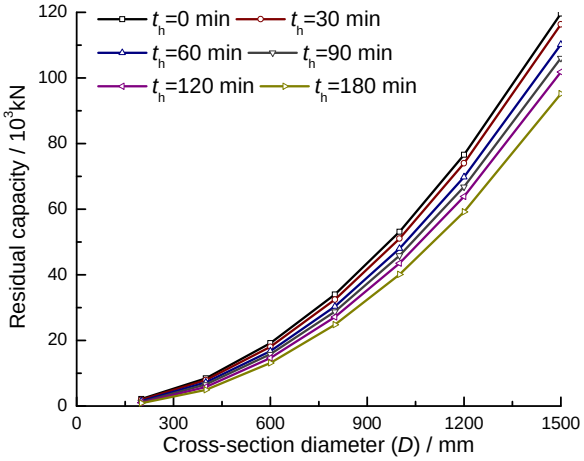
t_h=0 min
t_h=30 min
t_h=60 min
t_h=90 min
t_h=120 min
t_h=180 min
Residual capacity / 10^3kN
Cross-section diameter (D) / mm

(b)

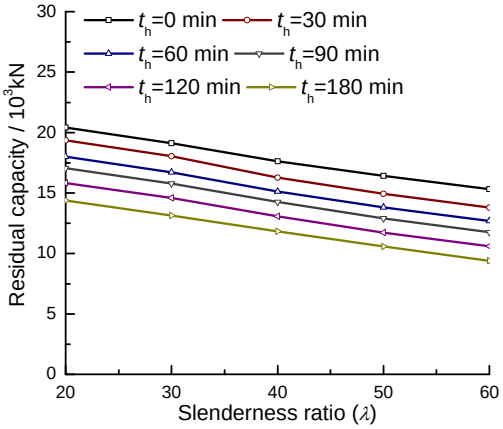
t_h=0 min
t_h=30 min
t_h=60 min
t_h=90 min
t_h=120 min
t_h=180 min
Residual capacity / 10^3kN
Slenderness ratio (λ)

(c)

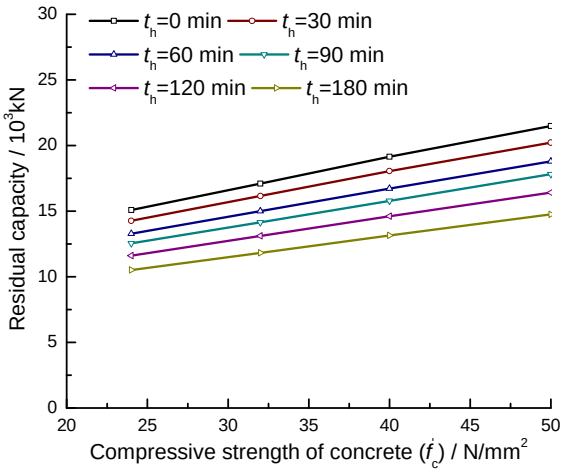
t_h=0 min
t_h=30 min
t_h=60 min
t_h=90 min
t_h=120 min
t_h=180 min
Residual capacity / 10^3kN
Compressive strength of concrete (f_c) / N/mm^2

(d)

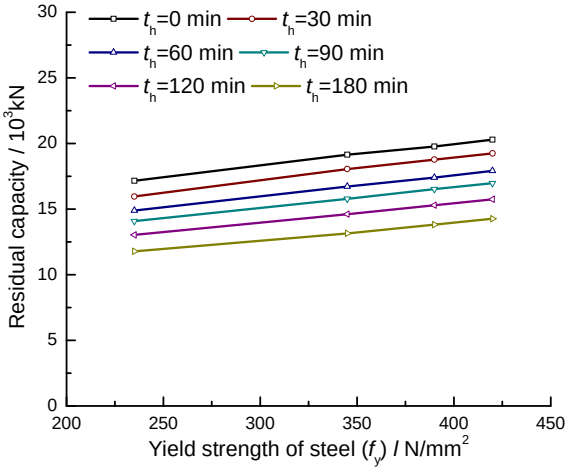
t_h=0 min
t_h=30 min
t_h=60 min
t_h=90 min
t_h=120 min
t_h=180 min
Residual capacity / 10^3kN
Yield strength of steel (f_y) / N/mm^2

(e)

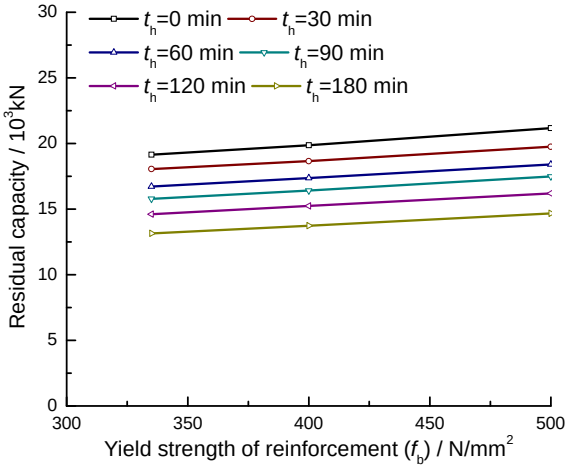
t_h=0 min
t_h=30 min
t_h=60 min
t_h=90 min
t_h=120 min
t_h=180 min
Residual capacity / 10^3kN
Yield strength of reinforcement (f_b) / N/mm^2

(f)

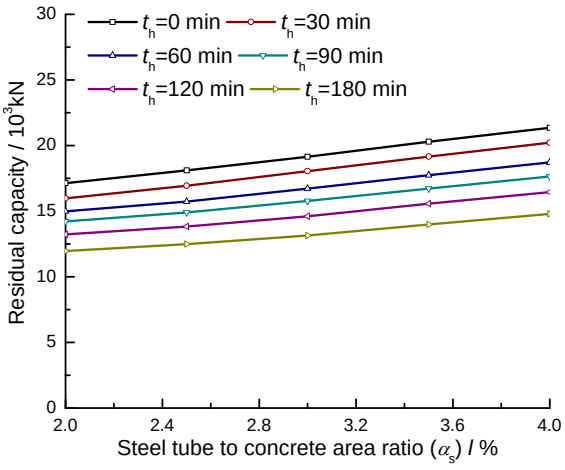

(g)

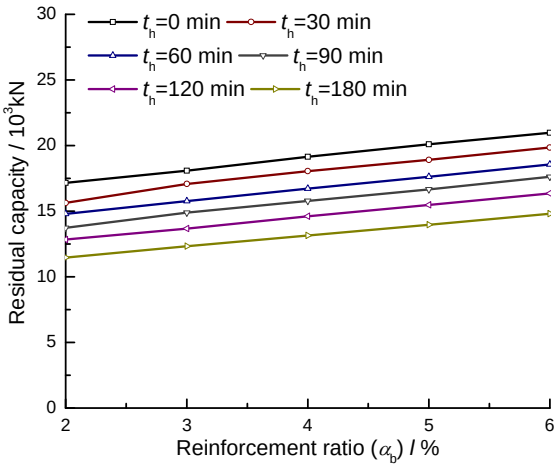

(h)

Fig.15 Influence of key parameters on residual capacity: (a) heating time; (b) cross-section diameter; (c) slenderness ratio; (d) compressive strength of concrete; (e) yield strength of steel; (f) yield strength of reinforcement; (g) steel tube to concrete area ratio; and (h) reinforcement ratio.

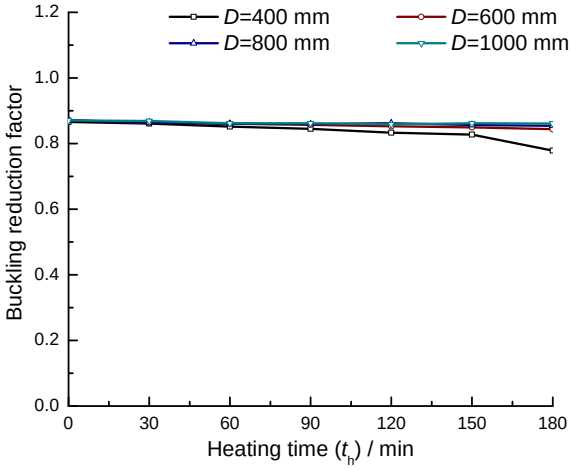
D=400 mm
D=600 mm
D=800 mm
D=1000 mm
Buckling reduction factor
Heating time (t_h) / min

(a)

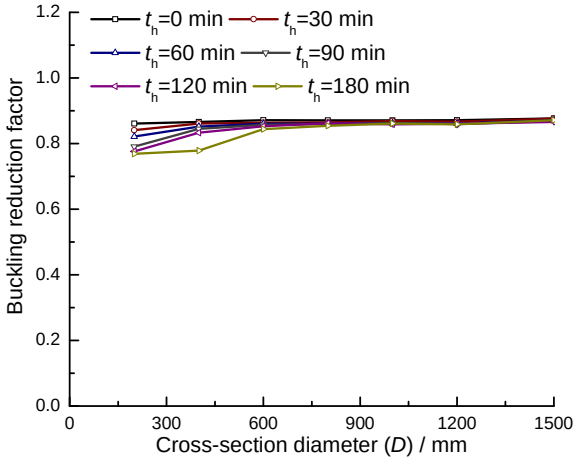
t_h=0 min
t_h=30 min
t_h=60 min
t_h=90 min
t_h=120 min
t_h=180 min
Buckling reduction factor
Cross-section diameter (D) / mm

(b)

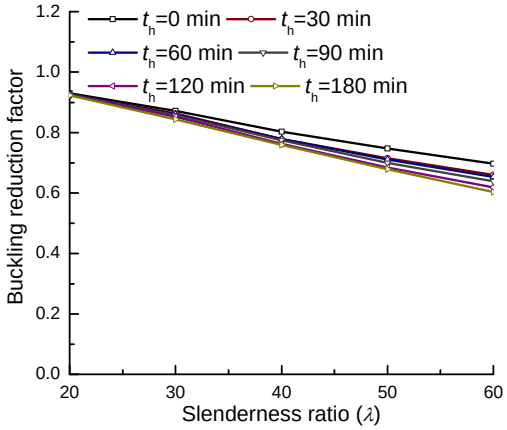
t_h=0 min
t_h=30 min
t_h=60 min
t_h=90 min
t_h=120 min
t_h=180 min
Buckling reduction factor
Slenderness ratio (λ)

(c)

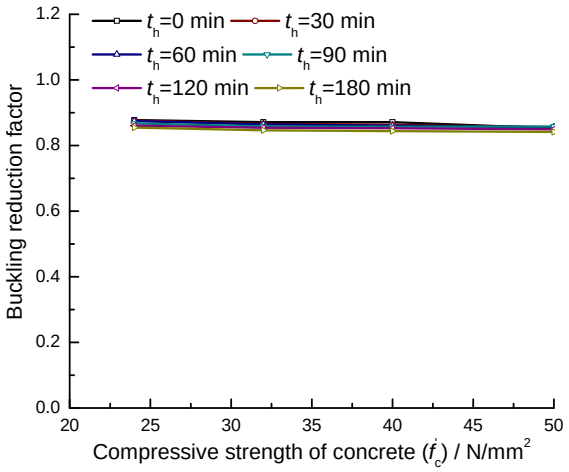
t_h=0 min
t_h=30 min
t_h=60 min
t_h=90 min
t_h=120 min
t_h=180 min
Buckling reduction factor
Compressive strength of concrete (f_c) / N/mm^2

(d)

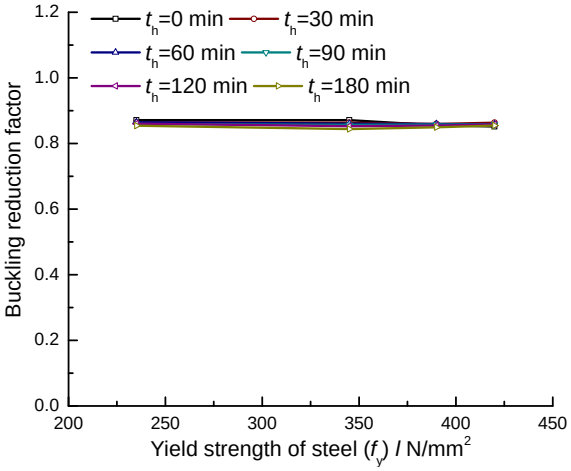
t_h=0 min
t_h=30 min
t_h=60 min
t_h=90 min
t_h=120 min
t_h=180 min
Buckling reduction factor
Yield strength of steel (f_y) / N/mm^2

(e)

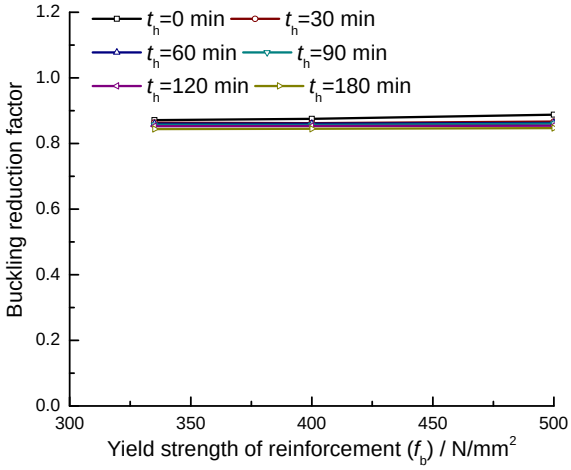
t_h=0 min
t_h=30 min
t_h=60 min
t_h=90 min
t_h=120 min
t_h=180 min
Buckling reduction factor
Yield strength of reinforcement (f_b) / N/mm^2

(f)

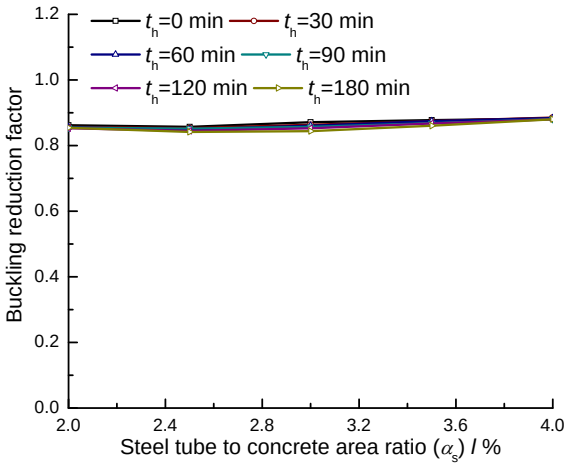

(g)

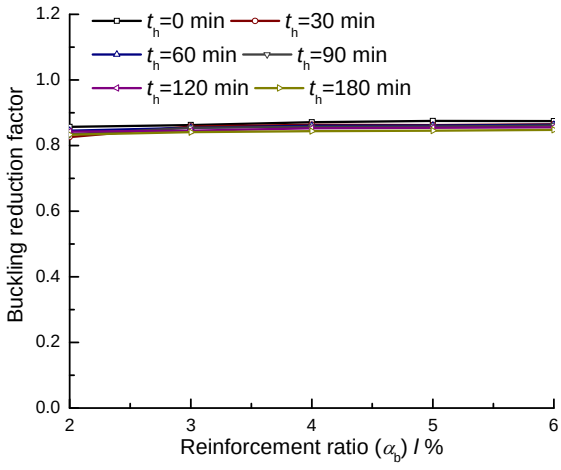

(h)

Fig.16 Influence of key parameters on buckling reduction factor: (a) heating time; (b) cross-section diameter; (c) slenderness ratio; (d) compressive strength of concrete; (e) yield strength of steel; (f) yield strength of reinforcement; (g) steel tube to concrete area ratio; and (h) reinforcement ratio.

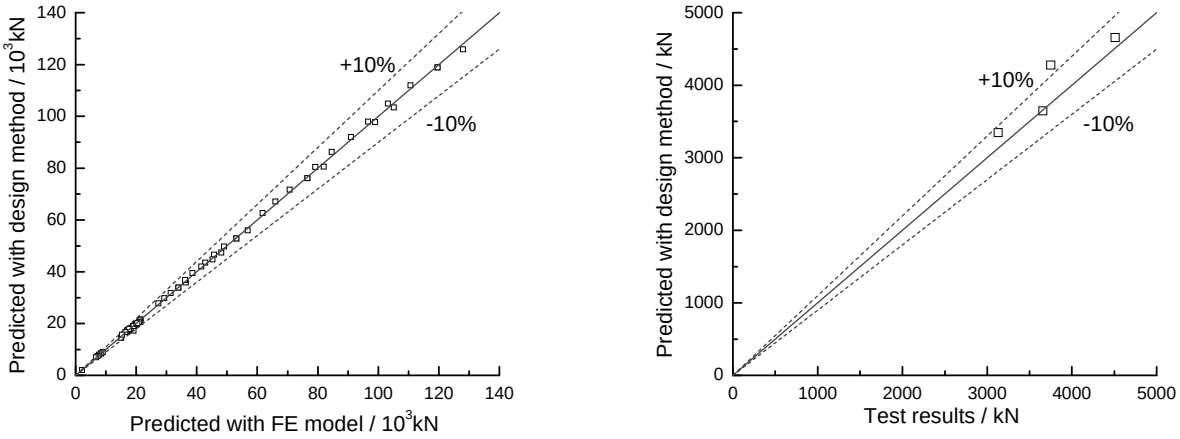

(a) (b)

Fig.17 Comparisons of predicted bearing capacities of STCRC slender columns which have not been exposed to fire: (a) between design method and FE model; and (b) between design method and test.

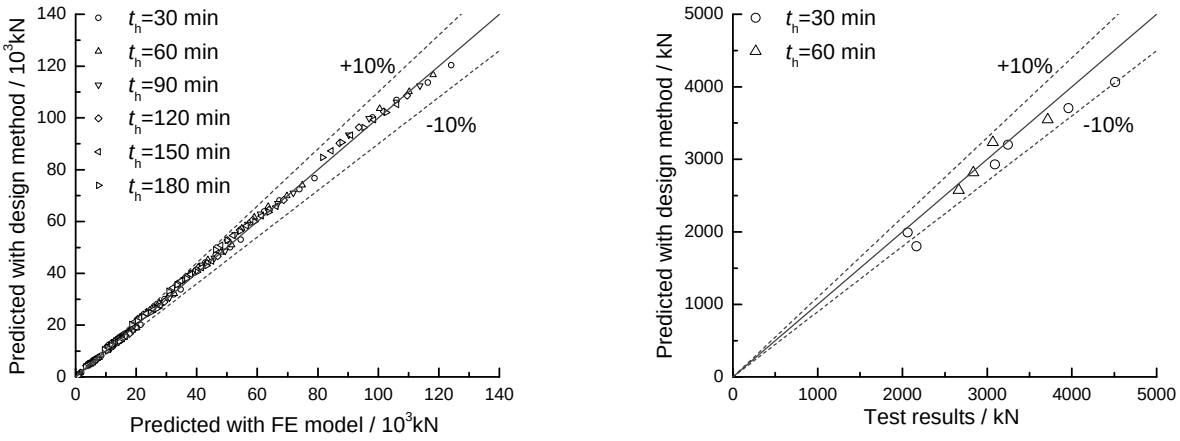

(a) (b)

Fig.18 Comparisons of predicted bearing capacities of STCRC slender columns after fire exposure: (a) between design method and FE model; and (b) between design method and test.

Table 1 Details of test specimens

Column No.	D (mm)		t_s (mm)		α_s (%)	L (mm)	Reinforcing Bars	α_b (%)	t_h (min)
	Norminal	Measured	Norminal	Measured					
C250-6-30-0	250	250.5	2.20	2.21	3.62	1500	6Φ20	3.98	0
C250-6-30-30	250	248.7	2.20	2.20	3.62	1500	6Φ20	3.98	30
C250-6-30-60	250	249.0	2.20	2.21	3.62	1500	6Φ20	3.98	60
C250-10-30-0	250	248.5	2.20	2.18	3.62	2400	6Φ20	3.98	0
C250-10-30-30	250	248.5	2.20	2.18	3.62	2400	6Φ20	3.98	30
C250-10-30-60	250	248.8	2.20	2.18	3.62	2400	6Φ20	3.98	60
C250-6-50-0	250	247.5	2.20	2.19	3.62	1500	6Φ20	3.98	0
C250-6-50-30	250	248.8	2.20	2.18	3.62	1500	6Φ20	3.98	30
C250-6-50-60	250	250.2	2.20	2.21	3.62	1500	6Φ20	3.98	60
C250-10-50-0	250	250.3	2.20	2.15	3.62	2400	6Φ20	3.98	0
C250-10-50-30	250	248.3	2.20	2.18	3.62	2400	6Φ20	3.98	30
C250-10-50-60	250	248.7	2.20	2.15	3.62	2400	6Φ20	3.98	60
C200-6-30-30	200	199.5	1.76	1.77	3.62	1200	6Φ16	3.98	30
C200-10-30-30	200	198.5	1.76	1.76	3.62	2000	6Φ16	3.98	30

Table 2 Ambient temperature properties of steel tube after fire exposure times of 0, 30 and 60 minutes

Norminal t_s (mm)	t_h (min)	E_s (N/mm^2)	f_y (N/mm^2)	f_{su} (N/mm^2)	v_s
1.76	0	1.99×10^5	342.9	488.8	0.263
2.20	0	1.98×10^5	318.9	424.9	0.304
1.76	30	1.87×10^5	341.5	445.7	0.292
2.20	30	2.07×10^5	295.2	378.1	0.294
2.20	60	1.82×10^5	262.1	327.9	0.281

Table 3 Properties of longitudinal reinforcing bars and stirrups

Steel type	Norminal d_s (mm)	E_b (N/mm^2)	f_b (N/mm^2)	f_{bu} (N/mm^2)
Hot-rolled plain	8.0	1.93×10^5	435.4	668.8
Hot-rolled ribbed	16.0	1.64×10^5	326.2	498.0
Hot-rolled ribbed	20.0	1.84×10^5	357.4	570.5

Table 4 Concrete cube strength and elastic modulus

Nominal f_{cu} (N/mm^2)	$f_{cu,28}$ (N/mm^2)	$E_{c,28}$ (N/mm^2)	$f_{cu,test}$ (N/mm^2)	$E_{c,test}$ (N/mm^2)	Age of concrete at test day (days)
30	33.7	2.52×10^4	53.8	-	184
50	63.6	3.63×10^4	76.3	3.72×10^4	289

Table 5 Circular CFST slender columns after ISO-834 standard fire [34]

Column No.	D (mm)	t_s (mm)	L (mm)	e (mm)	a (mm)	f_y (N/mm^2)	f_{cu} (N/mm^2)	t_h (min)
C1	108	4.32	600	0	0	356	71.3	90
C2	108	4.32	600	15	0	356	71.3	90
C3	108	4.32	1200	0	0	356	71.3	90
C4	108	4.32	1200	15	0	356	71.3	90
CP1	108	4.32	900	0	25	356	71.3	180
CP2	108	4.32	900	15	25	356	71.3	180

Table 6 Values of studied parameters

Parameter	Values	Fixed value
t_h (min)	0, 30, 60, 90, 120, 150, 180	-
D (mm)	200, 400, 600, 800, 1000, 1200, 1500	600
λ	20, 30, 40, 50, 60	30
f_c' (N/mm^2)	24, 32, 40, 50	40
f_y (N/mm^2)	235, 345, 390, 420	345
f_b (N/mm^2)	335, 400, 500	335
α_s (%)	2.0, 2.5, 3.0, 3.5, 4.0	3.0
α_b (%)	2.0, 3.0, 4.0, 5.0, 6.0	4.0